VolFe: an open-source Python package for calculating melt-vapor equilibria including silicate melt, carbon, hydrogen, sulfur, and noble gases

Ery C. Hughes: Te Pū Ao GNS Science (e.hughes@gns.cri.nz)
Philippa Liggins: University of Oxford
Penny Wieser: UC Berkeley
Edward M. Stolper: Caltech

This preprint is not an accepted peer-reviewed manuscript. A version of this preprint has been resubmitted to Volcanica following one round of peer-review.

VolFe: an open-source Python package for calculating melt-vapor equilibria including silicate melt, carbon, hydrogen, sulfur, and noble gases

Ery C. Hughes[1,2,*], Philippa Liggins[3], Penny Wieser[4], Edward M. Stolper[2]
[1]Te Pū Ao GNS Science, National Isotope Centre/Avalon, Lower Hutt 5010, Aotearoa New Zealand
[2]Division of Geological and Planetary Sciences, Caltech, Pasadena, CA 91125, USA
[3]Oxford Research Software Engineering Group, University of Oxford, 1–4 Keble Road, Oxford OX1 3NP, UK
[4]Earth and Planetary Science, UC Berkeley, Berkeley, CA, USA
*e.hughes@gns.cri.nz
ECH: 0000-0002-3445-281X
PL: 0000-0003-2880-6711
PW: 0000-0002-1070-8323
EMS: 0000-0001-8008-8804
Keywords: volatiles, thermodynamic, degassing, open-source, melt, vapor

Abstract

VolFe is an open-source flexible and adaptable thermodynamic framework in Python for calculating the equilibrium composition of melt and vapor. VolFe considers basaltic through rhyolitic melts including the volatiles carbon, hydrogen, sulfur, and the noble gases. VolFe models both reduced and oxidised systems due to the range of melt and vapor species included. Hence, VolFe is applicable to terrestrial (e.g., mid-ocean ridges to arcs) and extra-terrestrial (e.g., the Moon and Mars) systems. New parameterisations of "model-dependent variables" (e.g., volatile solubility functions, sulfide-saturation conditions, fugacity coefficients, etc.) can be added as new experimental studies come out, enhancing VolFe's future applicability. The main calculations currently included in VolFe are the pressure of vapor-saturation based on the dissolved volatile content of melts; H_2O-CO_2 isobars, open- and closed-system degassing and regassing; an oxybarometer based on the melt sulfur content; and uncertainty propagation of the input melt compositions on calculation outputs. As an example, we apply VolFe to melt inclusion and submarine pillow glass data from the Marianas arc.

1 Introduction

The behaviour of volatile elements such as carbon (C), hydrogen (H), sulfur (S), the noble gases (He, Ar, Ne, etc.), and the halogens (Cl, Br, etc.) during magmatic and volcanic processes is important in volcanology and igneous petrology. Exsolving vapor from degassing can provide a driving force for eruptions, leading to explosive or quiescent addition of volatiles to the atmosphere that can impact climate and/or human health (e.g., Marshall et al., 2022; Stewart et al., 2021). Surrounding country rocks can be altered by an exsolved fluid phase, sometimes playing a role in ore formation (e.g., Simon and Ripley, 2011). The loss of volatiles to vapor can also affect the physical properties, chemical compositions, and liquid lines of descent of magmas (e.g., Applegarth et al., 2013; Dingwell

et al., 1996). Additionally, the oxygen fugacity (f_{O2}) of the system can evolve during degassing because of the differing dominant oxidation states of volatile elements in coexisting melt and vapor (Anderson and Wright, 1972; Brounce et al., 2017; Burgisser and Scaillet, 2007; Candela, 1986; Carmichael and Ghiorso, 1986; Gaillard et al., 2015, 2011; Kelley and Cottrell, 2012; Métrich et al., 2009; Moussallam et al., 2014, 2016; Hughes et al., 2023).

A quantitative understanding of volatile degassing from magmas requires both studies of natural systems and physical and chemical models of degassing to aid in their interpretation (e.g., Papale et al., 2022). Consequently, there has been considerable interest in developing quantitative models of melt-vapor chemical equilibria for silicate melt-H_2O-CO_2, resulting in a range of applicable tools: e.g., VolatileCalc (Newman and Lowenstern, 2002); MagmaSat (Ghiorso and Gualda, 2015); Solwcad (Papale et al., 2006); and VESIcal (Iacovino et al., 2021). More recently, such tools include sulfur: e.g., CHOSETTO (Moretti et al., 2003; Moretti and Papale, 2004); an unnamed tool from Gaillard and others (e.g., Gaillard et al., 2011; Gaillard and Scaillet, 2014); SolEx (Witham et al., 2012); D-Compress (Burgisser et al., 2015); Evo (Liggins et al., 2022, 2020); MAGEC (Sun and Lee, 2022; Sun and Yao, 2024); Sulfur_X (Ding et al., 2023); MELTS (Ghiorso et al., 2023); Petrolog4[1]; and our tool that we now refer to as VolFe (Hughes et al., 2022, 2024). Despite differences in their details, these tools typically calculate the equilibrium state of melt-vapor systems given a set of independent variables (e.g., vapor saturation pressures and degassing paths). These tools have been used extensively to interpret natural sample data, such as the compositions of melt inclusions (e.g., Ranta et al., 2024; Werner et al., 2020; Wieser et al., 2021), submarine pillow glasses (e.g., Brounce et al., 2017; Lund et al., 2018; Soule et al., 2012), and volcanic gases (e.g., Aiuppa et al., 2022; Burton et al., 2023).

We note the distinction between individual solubility models for specific volatiles (e.g., eq. (1) and (8) for CO_2 or eq. (2) and (9) for H_2O solubility in basaltic melts in Dixon, 1997) – which we refer to as solubility functions in this paper – and these tools that model systems containing multiple volatiles by combining various solubility models. For instance, VolatileCalc is a tool that includes the CO_2 and H_2O solubility functions from Dixon (1997) and others. Sometimes a new study will produce both a new solubility function and a new tool: e.g., Ding et al. (2023) describe both a new solubility function for sulfur (their eq. (9) and (10) and Table 3) and a new tool called Sulfur_X for degassing calculations. Hence, sometimes these tools have their own unique solubility function, other times they incorporate solubility functions already available in the literature, or both.

In this paper we describe VolFe and its implementation via an open-source Python package for calculating melt-vapor equilibria (available at GitHub[2] and archived in Zenodo; *will add appropriate REF when created*). The name "VolFe" derives from "Volatile + Fe" to highlight the role and

[1] https://petrologsoftware.com/
[2] https://github.com/eryhughes/VolFe

evolution of f_{O2} for processes involving melt-vapor equilibria. Our goal is for VolFe to be user-friendly, flexible, adaptable, and to evolve over time as new thermochemical data become available and new applications are envisioned. This tool was initially developed and applied to modeling the sulfur solubility minimum and maximum in silicate melt ± vapor ± sulfide ± anhydrite assemblages for basaltic systems in which the vapor was restricted to S- and O-bearing species only (i.e., no C or H present in the system; Hughes et al., 2022) and to examine the influence of sulfur and f_{O2} on the pressure of vapor-saturation in magmas (P^{v}_{sat}; Hughes et al., 2024). Although the thermodynamic model was fully described in these papers, significant effort has been applied to making the underlying source code more accessible to the community (with the inclusion of documentation and examples), as well as expanding the range of possible calculations that can be performed (e.g., degassing including C, H, and S). The goal of this paper is to explain more fully the structure of the Python package and its capabilities, as well as the various assumptions and approximations that are used. To help with implementation by potential users (including those with little or no coding experience), we provide numerous examples of usage through Jupyter Notebooks and fuller documentation via ReadTheDocs[3].

2 Thermodynamic framework

We chose a simple thermodynamic approach to construct VolFe. The state of the system is calculated by assuming that chemical equilibrium is achieved given the values of the selected independent variables, where paths can be formed by sequential steps of these calculations (e.g., decreasing P would result in degassing). Chemical equilibrium is described by a set of chemical reactions: (1) among species within the melt or vapor phase (i.e., homogeneous equilibria), and (2) between species in the melt and vapor (i.e., heterogeneous equilibria). All these reactions must be linearly independent, meaning none of these reactions can be created by adding or subtracting combinations of the other reactions. Each chemical reaction has an equilibrium constant that constrains the relative concentrations of the reactants and products at equilibrium given the independent variables.

To use this approach, we first choose the phases that might be present and the species within them. Then we choose a set of linearly independent equilibria that relate the species within and between the different phases. We refer to this as the thermodynamic framework of the system (Section 3). The number of independent equilibria (E) required to describe the system is determined by:

$$E = N - c, \tag{1}$$

[3] https://volfe.readthedocs.io/en/latest/

where N is the total number of species in the system (e.g., the total number of species in the melt and vapor phases) and c is the number of components required to describe possible variations in the composition of the whole system regardless of the actual speciation (Prigogine and Defay, 1954; e.g., Section 3.1). This framework is only as good as its inventory of potential phases, species, and chemical reactions (i.e., thermochemical parameters). Thus, if there are key melt or vapor species in the system of interest to a particular problem that are currently not included in VolFe (e.g., the halogens), the results from VolFe will not be appropriate. However, the inclusion of oxidised *and* reduced species (e.g., H_2O and H_2; CO_2 and CO_{mol}, etc.: Section 3) in the melt and vapor means magmas over a wide range of f_{O2} can be modelled: from reduced lunar or martian basalts to oxidised arc basalts. Additionally, various combinations of volatiles allow different systems to be modelled, from terrestrial magmas with CHOS-bearing volatiles to magmas on Io with only S-O-bearing volatiles.

The values of the thermochemical parameters embedded in VolFe depend on the parameterisation chosen to evaluate them at a given set of conditions, which we term "model-dependent variables" (Section 3). These variables include equilibrium constants, solubility functions, fugacity coefficients, definitions of f_{O2} buffers, etc. They are termed "model-dependent" because different parameterisations to calculate these variables are available in the literature. For instance, the absolute f_{O2} value of the Fayalite-Magnetite-Quartz (FMQ) buffer at a certain P and temperature (T) can be calculated using the parameterisation of Frost (1991) or O'Neill (1987), etc. Hence, the FMQ buffer is a model-dependent variable. Similarly, different parameterizations for the solubility functions of H_2O, CO_2, etc. in volatile-bearing melts (e.g., Dixon, 1997; Dixon et al., 1995; Ghiorso and Gualda, 2015; Iacono-Marziano et al., 2012) and of the fugacity coefficients for species in the vapor phase (e.g., Belonoshko and Saxena, 1992; Holland and Powell, 1991; Holloway, 1977; Shi and Saxena, 1992) exist in the literature. In VolFe, we have included various parameterisations from the literature of these model-dependent variables that can be chosen by the user when running calculations, and new ones can be added as desired. For example, if the parameterisations of the solubility function for H_2 currently available in VolFe (Table S8) are not appropriate for a user's system of interest (e.g., either because of new data or to account for their variability as a function of the major element composition of the melt), a new parameterisation could be added (see example in the ReadTheDocs). Where possible, the functions currently available in VolFe to calculate these parameterisations have been benchmarked against the original publication (e.g., results described in the text, figures, or tables in the original paper; supplemental calculators provided as supporting spreadsheets; or other codes). These benchmarking results are shown in the ReadTheDocs and highlighted in Tables S1–11. The goal is to make VolFe adaptable as new parameterisations become available, especially as new experiments are conducted.

Finally, to calculate the state of the system at equilibrium either statically or along a particular path, we require the choice of a set of independent variables whose values we specify for the

calculation or at each step along the path. If the relative proportions of the phases are not required (e.g., at P^{v}_{sat}; Hughes et al., 2024), the phase rule dictates the number of independent intensive variables (i.e., the variance, F) required to specify the state of the system for a given number of phases (φ) and components (Gibbs, 1978, 1976):

$$F = c + 2 - \varphi. \quad (2)$$

Alternatively, if the equilibrium proportions of the phases are required (e.g., for modelling degassing) we use Duhem's theorem. This states that for a closed-system (i.e., where the masses of all components remain constant and are known), the equilibrium state is completely determined once the values of any two independent intensive and/or extensive variables are specified (e.g., Prigogine and Defay, 1954; Powell et al., 1998). The constancy of the bulk composition of the system to apply Duhem's theorem requires mass balancing all components across all phases present in each step on any specified path (Section 3.3).

Whether the phase rule or Duhem's theorem is the basis for the number and nature of the chosen independent variables, different choices of these variables enable different types of calculations. VolFe contains functions to calculate the state of the system at equilibrium given several choices of independent variables (Section 4). These include the pressure of vapor-saturation for a given volatile-bearing melt composition and T (P^{v}_{sat}, Section 4.1); CO_2–H_2O isobars for a given volatile-free melt composition and T (Section 4.2); the composition of melt and vapor during closed- and open-system degassing or regassing (Section 4.3); and estimating f_{O2} from the sulfur content in the melt (Section 4.4). For calculations currently available in VolFe, T is always an independent variable and paths are currently isothermal. Alternative choices of the independent variables defining a calculation can be added according to the problem to be solved, allowing flexibility.

3 Phases, species, chemical reactions, and model-dependent variables

The implementation of VolFe given here is essentially that described in Hughes et al. (2024b) with a few updates (Figure 1). We outline currently available parameterisations of model-dependent variables (e.g., equilibrium constants, fugacity coefficients, etc.) in VolFe (Tables S1–10**Error! Reference source not found.**); interested readers should check the ReadTheDocs for the most up-to-date list. The specific parameterisation for each model-dependent variable can be chosen by the user when running calculations in VolFe.

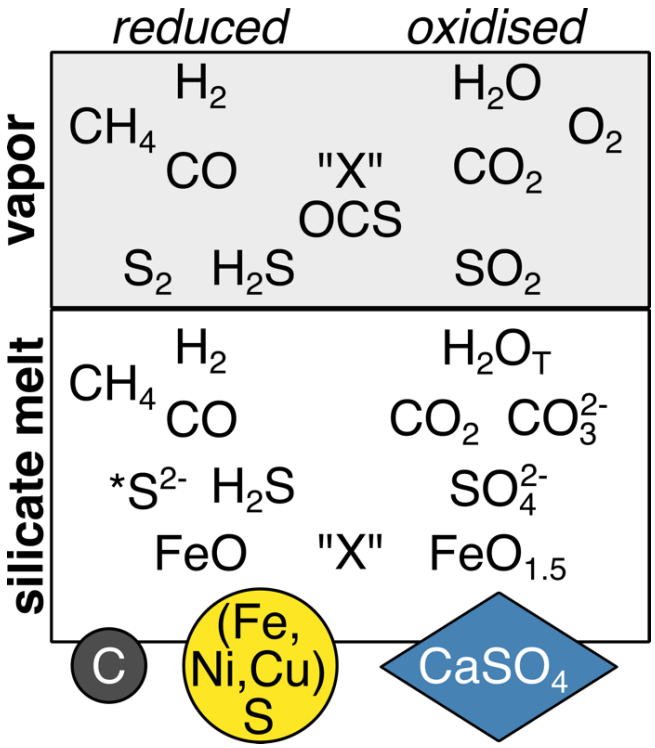

Figure 1. Phases and species considered in the thermodynamic framework of VolFe. Generally, reduced species are to the left and oxidised species are to the right. "X" represents a non-reactive molecular volatile species, such as a noble gas. Along the bottom, the small dark-grey circle represents graphite; the large yellow circle liquid sulfide; and the blue diamond anhydrite.

VolFe is primarily focused on the two-phase coexistence of melt and vapor (i.e., $\varphi = 2$). We use the term vapor throughout to describe the lower density fluid that may coexist with silicate melt, although super-critical fluid is more appropriate under certain conditions. VolFe can also test for saturation with sulfide melt, anhydrite, and/or graphite (see Section 3.6 for further details), but crystallisation of silicate or oxide minerals is not currently considered. The bulk composition of systems currently included in VolFe comprise three to six components ($3 < c < 6$): (1) a silicate component, which is defined by the volatile-free composition of the silicate melt and includes all iron as FeO (FeO_T) and all other non-volatile oxides: SiO_2, Al_2O_3, TiO_2, MnO, MgO, CaO, Na_2O, K_2O, and P_2O_5 (e.g., Hughes et al., 2024, 2022); (2) the amount of oxygen (O) in excess of the silicate component; and (3–6) at least one of C, H, S, and/or "X". Note that O contained in the silicate component cannot exchange between the melt and vapor. The O that can exchange between the melt and the vapor is contained in the "O in excess of the silicate component": this includes O contained in the vapor; O associated with iron in excess of that already in the silicate component as the silicate component is defined using FeO only; and/or O associated with volatile species in the melt (e.g., Hughes et al., 2023). For molecular melt species (i.e., CO, $CO_{2,mol}$), all O present in the species is counted towards the excess O. For the ionic melt species (CO_3^{2-} and SO_4^{2-}), all but one of the oxygens is counted towards the excess O – the final O is associated with silicate component (e.g., CaO, Na_2O),

which does not exchange between the melt and vapor (i.e., they are treated as CO_2 and SO_3). All O present in H_2O_T is included in the O budget. "X" represents a non-reactive, molecular volatile species – such as a noble gas – and its chemical identity is governed by its molecular mass, fugacity coefficient, and solubility function (described in the sub-sections below). Currently "X" can be either Ar or Ne in VolFe.

The species present in the melt and vapor (Sections 3.1 and 3.2) are selected automatically by VolFe based on which volatiles are present in non-zero concentrations for the user-specified composition. Certain melt and vapor species can be excluded if required: e.g., treating H_2, CO, CH_4, and/or H_2S as completely insoluble in the melt or assuming these species are not present in the vapor. There are some limitations on the combinations of species possible (e.g., currently, the re/degassing calculation, cannot have both S and "X" present in the bulk composition).

3.1 Vapor

The vapor has a bulk composition described by five components (C, O, H, S, and "X") and currently includes 11 chemical species (Figure 1): O_2, H_2, CO, S_2, H_2O, CO_2, SO_2, CH_4, OCS, H_2S, and "X". These vapor species are related through six, linearly independent, homogeneous vapor equilibria (eq. 3–8, Table 1). Each homogenous vapor reaction has an equilibrium constant (K) that depends only on T. Although others could be added, currently only a single parameterisation for each K is available in VolFe from Moussallam et al. (2019), O'Neill and Mavrogenes (2022), and Ohmoto and Kerrick (1977), which have been benchmarked where possible (further details are available in Table S1).

Table 1. Homogeneous vapor equilibria considered in VolFe.

Reaction among vapor species	Equilibrium constant ($K_{X(Y)}$)	Eq. no.
$H_2 + 0.5O_2 \rightleftarrows H_2O$	$K_{\mathrm{H}}(T) = \frac{f_{\mathrm{H_2O}}}{f_{\mathrm{H_2}} f_{\mathrm{O_2}}^{0.5}}$	(3)
$CO + 0.5O_2 \rightleftarrows CO_2$	$K_{\mathrm{C}}(T) = \frac{f_{\mathrm{CO_2}}}{f_{\mathrm{CO}} f_{\mathrm{O_2}}^{0.5}}$	(4)
$0.5S_2 + O_2 \rightleftarrows SO_2$	$K_{\mathrm{S}}(T) = \frac{f_{\mathrm{SO_2}}}{f_{\mathrm{S_2}}^{0.5} f_{\mathrm{O_2}}}$	(5)
$CH_4 + 2O_2 \rightleftarrows CO_2 + 2H_2O$	$K_{\mathrm{CH}}(T) = \frac{f_{\mathrm{CO_2}} f_{\mathrm{H_2O}}^2}{f_{\mathrm{CH_4}} f_{\mathrm{O_2}}^2}$	(6)

$0.5S_2 + H_2O \rightleftarrows H_2S + 0.5O_2$	$K_{HS}(T) = \frac{f_{H_2S} f_{O_2}^{0.5}}{f_{S_2}^{0.5} f_{H_2O}}$	(7)
$OCS + 2CO_2 \rightleftarrows 3CO + SO_2$	$K_{SC}(T) = \frac{f_{CO}^3 f_{SO_2}}{f_{CO_2}^2 f_{OCS}}$	(8)

Notes: $K_{X(Y)}(T)$ is the equilibrium constant involving component X and additionally Y where relevant (oxygen is always involved and therefore not indicated: e.g., K_{SC} is for S- and C-bearing vapor species) and f_i is the fugacity of species *i*.

The partial pressure (p_i), mole fraction (x_i^v), and fugacity (f_i) for each vapor species (i) are related by:

$$p_i = \frac{f_i}{\gamma_i^v} = x_i^v P \,, \tag{9}$$

(eq. 3.20 in Denbigh, 1971), where γ_i^v is the fugacity coefficient. We treat the vapor as an ideal mixture of non-ideal gases (i.e., the Lewis-Randall rule; eq. 3.72 in Denbigh, 1971) such that the γ_i^v of each vapor species depends on *P* and *T* but not on the vapor composition. This is a common simplification used in many melt-vapor equilibria tools (e.g., VolatileCalc, DCompress, Sulfur_X, MAGEC, etc.) and given current uncertainties, the added complexity of modelling a non-ideal mixture of non-ideal gases does not seem necessary (Iacovino, 2015). Currently available parameterisations in VolFe of γ_i^v are from Shaw and Wones (1964), Shi and Saxena (1992) (including modifications described in Hughes et al. 2024, 2022), Holland and Powell (1991), and Flowers (1979) correction to Holloway (1977) modified from MIMiC (Rasmussen et al., 2021) and originally from VolatileCalc (Newman & Lowenstern, 2001); which have been benchmarked where possible (Table S2). Additionally, VolFe can treat any vapor species as ideal (i.e., $\gamma_i^v = 1$). At equilibrium, the sum of the partial pressures of all the vapor species equals the total pressure of the system (eq. 3.21 in Denbigh, 1971):

$$P = \sum_{i=1}^{n} p_i = P_{\text{sat}}^v. \tag{10}$$

3.2 Volatile solubility in the melt

The whole system (i.e., melt and vapor) is described by six components: C, O, H, S, "X", plus the volatile-free silicate component in which all Fe is present as FeO. VolFe currently includes ten volatile-bearing chemical species in the melt (Figure 1): molecular H_2 ($H_{2,mol}$), H_2O_T (all oxidised hydrogen: the combination of OH^- and H_2O_{mol}), molecular CO (CO_{mol}), carbonate ions (CO_3^{2-}), molecular CO_2 ($CO_{2,mol}$), molecular CH_4 ($CH_{4,mol}$), sulfide ions other than H_2S ($*S^{2-}$), sulfate ions

(SO_4^{2-}), molecular H_2S (H_2S_{mol}), and an inert molecular element ("X"$_{mol}$). There are two additional, volatile-free silicate melt "species": FeO and $FeO_{1.5}$ (Figure 1). The heterogeneous melt-vapor equilibria describing volatile solubility in the melt are listed in Table 2 and derived in full in the Supplementary Material of Hughes et al. (2024).

Table 2. Heterogeneous melt-vapor equilibria considered in VolFe.

Solubility mechanism	Solubility function	Eq. no.
$H_2(v) \rightleftarrows H_{2,mol}(m)$	$f_{H_2} = \frac{w^m_{H_{2,mol}}}{C_{H_{2,mol}}}$	(11)
$H_2O(v) \rightleftarrows H_2O_T(m)$	$f_{H_2O} \approx \frac{\left(x^m_{H_2O_T}\right)^2}{C_{H_2O_T}}$	(12)
$CO(v) \rightleftarrows CO_{mol}(m)$	$f_{CO} = \frac{w^m_{CO_{mol}}}{C_{CO_{mol}}}$	(13)
$CO_2(v) \rightleftarrows CO_{2,T}(m)$	$f_{CO_2} = \frac{x^m_{CO_{2,T}}}{C_{CO_{2,T}}}$	(14)
$CH_4(v) \rightleftarrows CH_{4,mol}(m)$	$f_{CH_4} = \frac{w^m_{CH_{4,mol}}}{C_{CH_{4,mol}}}$	(15)
$0.5S_2(v) + O^{2-}(m) \rightleftarrows {}^*S^{2-}(m) + 0.5O_2(v)$	$f_{S_2} = \left(\frac{w^m_{{}^*S^{2-}}}{C_{{}^*S^{2-}}}\right)^2 f_{O_2}$	(16)
$0.5S_2(v) + 1.5O_2(v) + O^{2-}(m) \rightleftarrows SO_4^{2-}(m)$	$f_{S_2} = \left(\frac{w^m_{SO_4^{2-}}}{C_{SO_4^{2-}}}\right)^2 f_{O_2}^{-3}$	(17)
$H_2S(v) \rightleftarrows H_2S_{mol}(m)$	$f_{H_2S} = \frac{w^m_{H_2S_{mol}}}{C_{H_2S_{mol}}}$	(18)
"X"$(v) \rightleftarrows$ "X"(m)	$f_{"X"} = \frac{w^m_{"X"}}{C_{"X"}}$	(19)

Notes: v = vapor; m = melt; mol = molecular; f_i = fugacity of species i; x^m_i = mole fraction or w^m_i = concentration (depending on the units) of species i in the melt; C_i = the solubility function for species i, which is the constant of proportionality between the fugacity(ies) and the mole fraction/concentration of species i in the melt; ${}^*S^{2-}$ = sulfide associated with cations in the silicate melt, rather than associated with H, i.e., H_2S_{mol}. The units of the solubility functions for H_2, CO, CH_4, H_2S, and "X" use ppm by weight (ppmw) in the melt for concentration and bars for the fugacity in the vapor. The solubility functions for H_2O_T and $CO_{2,T}$ relate the mole fraction of H_2O_T or $CO_{2,T}$ in the melt (ignoring S and "X") to the fugacity of H_2O or

CO_2 in the vapor in bars, respectively: $x_i^m = (w_i^m/M_i)/\left(\left(w_{\mathrm{CO_{2,T}}}^m/M_{\mathrm{CO_2}}\right) + \left(w_{\mathrm{H_2O_T}}^m/M_{\mathrm{H_2O}}\right) + \left((1 - w_{\mathrm{CO_{2,T}}}^m - w_{\mathrm{H_2O_T}}^m)/M_m\right)\right)$, where w_i^m is the weight fraction of species *i* in the melt; and M_i is the molecular mass of species *i*. The molecular mass of the melt (M_m) is of the volatile-free silicate melt composition on a single-oxygen basis as described in Dixon et al. (1995).

Depending on the silicate melt composition, CO_2 can dissolve dominantly as CO_2 molecules ($CO_{2,mol}$) and/or as carbonate ions (CO_3^{2-}) formed by reaction with the silicate-dominated molecular framework of the melt (e.g., Behrens et al., 2004; Botcharnikov et al., 2006; Brooker et al., 1999; Fine and Stolper, 1986, 1985). However, the total amount of carbon dissolved as oxidised species (i.e., $CO_{2,T} = CO_{2,mol}$ and CO_3^{2-}) in any given melt composition is approximately proportional to f_{CO2} regardless of the relative amount of $CO_{2,mol}$ and CO_3^{2-} in the melt (e.g., Stolper et al., 1987; full derivation in the Supplementary Material of Hughes et al., 2024b). Hence, we have chosen to use a single heterogeneous melt-vapor equilibrium (eq. 14 in Table 2) combined with a homogeneous melt equilibria between $CO_{2,mol}$ and CO_3^{2-} to speciate $CO_{2,T}$ in the melt (e.g., Botcharnikov et al., 2006; Stolper et al., 1987; eq. 20 in Table 3).

Table 3. Additional equilibria considered in VolFe.

Reaction	Eq. no.
$CO_{2,mol}(m) + O^{2-}(m) \rightleftarrows CO_3^{2-}(m)$	(20)
$FeO(m) + 0.25O_2(v) \rightleftarrows FeO_{1.5}(m)$	(21)

Water is known to dissolve in silicate melt as both molecular H_2O (H_2O_{mol}) and hydroxyl ions (OH^-) (e.g., Burnham and Davis, 1974; Dixon et al., 1995; Lesne et al., 2011; Mysen et al., 1980; Stolper, 1982b). However, as in Hughes et al. (2024), we use Sievert's law as an approximation for the solubility of H_2O in the melt (i.e., eq. 12 in Table 2), which is a convenient and widely-used approximation appropriate up to ~6.4 wt% H_2O_T (e.g., Burnham, 1979; Ghiorso and Gualda, 2015; Stolper, 1982).

In many cases, people are interested in sub-systems of the full system illustrated in Figure 1, in which case the number of linearly independent statements of equilibria reduces. For example, suppose the system of interest contained negligible sulfur. Then we could remove all the sulfur-bearing species and their associated linearly independent equations. This is done automatically in VolFe if the volatile concentration of a particular component is 0.

3.3 Mass balance

When using Duhem's theory (e.g., for degassing calculations), mass must be conserved for all components within the system. Mass balance for each component distributed between melt and vapor is given by (e.g., Burgisser et al., 2015; Liggins et al., 2020):

$$w_i^T = M_i\left(w_v^{\mathrm{T}}\left(\left(\frac{n_i^v}{m_v^T}\right) - n_i^m\right) + n_i^m\right), \tag{22}$$

where i refers to the i^{th} component (i.e., C, H, S, O, or "X"); w_i^T is the total weight fraction of this component in the system; M_i is the molar mass of i; w_v^{T} is the weight fraction of vapor in the system; n_i^j is the moles of i in phase j; and m_v^T is the mass of the vapor defined as:

$$\begin{aligned} m_v^T = {} & M_{\mathrm{O_2}}x_{\mathrm{O_2}}^v + M_{\mathrm{H_2}}x_{\mathrm{H_2}}^v + M_{\mathrm{H_2O}}x_{\mathrm{H_2O}}^v + M_{\mathrm{CO}}x_{\mathrm{CO}}^v + M_{\mathrm{CO_2}}x_{\mathrm{CO_2}}^v + M_{\mathrm{CH_4}}x_{\mathrm{CH_4}}^v \\ & + M_{\mathrm{S_2}}x_{\mathrm{S_2}}^v + M_{\mathrm{SO_2}}x_{\mathrm{SO_2}}^v + M_{\mathrm{H_2S}}x_{\mathrm{H_2S}}^v + M_{\mathrm{OCS}}x_{\mathrm{OCS}}^v \end{aligned} \tag{23}$$

For carbon, i = C and in the vapor:

$$n_{\mathrm{C}}^v = x_{\mathrm{CO_2}}^v + x_{\mathrm{CO}}^v + x_{\mathrm{CH_4}}^v + x_{\mathrm{OCS}}^v, \tag{24}$$

where x_{j}^v is the mole fraction of species j in the vapor. In the melt:

$$n_{\mathrm{C}}^m = \frac{w_{\mathrm{CO_{2,T}}}^m}{M_{\mathrm{CO_{2,T}}}} + \frac{w_{\mathrm{CH_4}}^m}{M_{\mathrm{CH_4}}} + \frac{w_{\mathrm{CO}}^m}{M_{\mathrm{CO}}}. \tag{25}$$

For hydrogen, i = H:

$$n_{\mathrm{H}}^v = x_{\mathrm{H_2O}}^v + x_{\mathrm{H_2}}^v + 2x_{\mathrm{CH_4}}^v + x_{\mathrm{H_2S}}^v, \tag{26}$$

$$n_{\mathrm{H}}^m = \frac{w_{\mathrm{H_2O_T}}^m}{M_{\mathrm{H_2O}}} + \frac{w_{\mathrm{H_2}}^m}{M_{\mathrm{H_2}}} + \frac{2w_{\mathrm{CH_4}}^m}{M_{\mathrm{CH_4}}} + \frac{w_{\mathrm{H_2S}}^m}{M_{\mathrm{H_2S}}}. \tag{27}$$

In the case of H, a factor of 2 is applied to the right-hand side of eq. (22) as the component is treated as H_2.

For sulfur, i = S:

$$n_{\mathrm{S}}^v = x_{\mathrm{SO_2}}^v + 2x_{\mathrm{S_2}}^v + x_{\mathrm{H_2S}}^v + x_{\mathrm{OCS}}^v, \tag{28}$$

$$n_{\mathrm{S}}^m = \frac{w_{\mathrm{SO_4^{2-}}}^m}{M_{\mathrm{SO_4^{2-}}}} + \frac{w_{*\mathrm{S^{2-}}}^m}{M_{*\mathrm{S^{2-}}}} + \frac{w_{\mathrm{H_2S}}^m}{M_{\mathrm{H_2S}}}. \tag{29}$$

For oxygen i = O, such that:

$$n_{\mathrm{O}}^{v} = 2x_{\mathrm{O}_2}^{v} + 2x_{\mathrm{CO}_2}^{v} + x_{\mathrm{CO}}^{v} + x_{\mathrm{OCS}}^{v} + x_{\mathrm{H_2O}}^{v} + 2x_{\mathrm{SO}_2}^{v}, \tag{30}$$

$$n_{\mathrm{O}}^{m} = \frac{2w_{\mathrm{CO}_{2,\mathrm{T}}}^{m}}{M_{\mathrm{CO}_{2,\mathrm{T}}}} + \frac{w_{\mathrm{CO}}^{m}}{M_{\mathrm{CO}}} + \frac{w_{\mathrm{H_2O_T}}^{m}}{M_{\mathrm{H_2O}}} + \frac{3w_{\mathrm{SO}_4^{2-}}^{m}}{M_{\mathrm{SO}_4^{2-}}} + \frac{w_{\mathrm{Fe}}^{T}}{M_{\mathrm{Fe}}}\left(\frac{1.5\left(\frac{\mathrm{Fe}^{3+}}{\mathrm{Fe}^{2+}}\right)+1}{\left(\frac{\mathrm{Fe}^{3+}}{\mathrm{Fe}^{2+}}\right)+1}\right). \tag{31}$$

Note that SO_4^{2-} only contributes three oxygen's as the fourth O is part of the silicate component. The Fe-term in eq. (31) is not included in the first n_{O}^{m}-term in eq. (22) because Fe is not present in the vapor.

And for species "X", *i* = "X":

$$n_{\mathrm{"X"}}^{v} = x_{\mathrm{"X"}}^{v}, \tag{32}$$

$$n_{\mathrm{"X"}}^{m} = \frac{w_{\mathrm{"X"}}^{m}}{M_{\mathrm{"X"}}}. \tag{33}$$

3.4 Solubility functions and their dependence on *P, T,* and melt composition

The formulations and parameterisations of the solubility functions in Table 2 as functions of *P*, *T*, and melt composition are key to the quantification of melt-vapor equilibria using VolFe. As in Hughes et al. (2024), we use the broad term "solubility function" rather than the thermodynamically rigorous "equilibrium constant".

As an example, we consider the dissolution of S_2 from the vapor into the melt as $*S^{2-}$ (all sulfide dissolved in the melt apart from H_2S_{mol}) based on the solubility mechanism given in Table 2 as eq. (17). We can write the equilbrium constant for this reaction ($K_{*\mathrm{S}^{2-}}$) as:

$$K_{*\mathrm{S}^{2-}}(P,T) = a_{*\mathrm{S}^{2-}}^{m}\left(\frac{f_{\mathrm{O}_2}}{f_{\mathrm{S}_2}}\right)^{0.5} = \gamma_{*\mathrm{S}^{2-}}^{m} w_{*\mathrm{S}^{2-}}^{m}\left(\frac{f_{\mathrm{O}_2}}{f_{\mathrm{S}_2}}\right)^{0.5}, \tag{34}$$

where $a_{*\mathrm{S}^{2-}}^{m}$ is the activity of the $*S^{2-}$ species in the melt; f_i is the fugacity of species *i* in the coexisting vapor; $\gamma_{*\mathrm{S}^{2-}}^{m}$ is the activity coefficient of species $*S^{2-}$ in the melt; and $w_{*\mathrm{S}^{2-}}^{m}$ is the concentration (as weight fraction) of the $*S^{2-}$ species in the melt. The equilbrium constant, $K_{*\mathrm{S}^{2-}}$, is a function only of *P* and *T* – not melt composition – yet the solubility of the $*S^{2-}$ species in silicate melts is strongly compositionally dependent (e.g., Fincham and Richardson, 1954), reflecting the strong compositional dependence of the activity coefficients in eq. (34).

One option is that the overall effects of melt composition are incorporated into the $\gamma_{*\mathrm{S}^{2-}}^{m}(P,T,X)$ function and thus also into the solubility function:

$$C_{*S^{2-}}(P,T,X) = \frac{K_{*S^{2-}}(P,T)}{\gamma^m_{*S^{2-}}(P,T,X)} = w^m_{*S^{2-}}\left(\frac{f_{O_2}}{f_{S_2}}\right)^{0.5}, \quad (35)$$

where C_{*S2-} is the solubility function for $*S^{2-}$ and the X refers to melt composition. Alternatively, C_i is treated as a capacity, as is commonly used for sulfide and sulfate (e.g., Fincham & Richardson, 1954; O'Neill 2021, Spera & Bergman, 1980). In other words, a separate equilibrium constant can be written for the reaction between $*S^{2-}$ and each of the oxide components in the melt:

$$0.5S_2(v) + CaO(m) \rightleftarrows CaS(m) + 0.5O_2(v) \qquad K^{CaO}_{*S^{2-}}(P,T) = \frac{w^m_{CaS}}{w^m_{CaO}}\left(\frac{f_{O_2}}{f_{S_2}}\right)^{0.5}, \quad (36)$$

$$0.5S_2(v) + FeO(m) \rightleftarrows FeS(m) + 0.5O_2(v) \qquad K^{FeO}_{*S^{2-}}(P,T) = \frac{w^m_{FeS}}{w^m_{FeO}}\left(\frac{f_{O_2}}{f_{S_2}}\right)^{0.5}, \quad (37)$$

etc.

The capacity is then the concentration-weighted sum of the K_i's for each component (e.g., Fincham and Richardson, 1954; O'Neill, 2021; Spera and Bergman, 1980):

$$\begin{aligned} C_{*S^{2-}}(P,T,X) &= \sum_{i=1}^{n} w_i^m \cdot K^i_{*S^{2-}}(P,T) \\ &= w^m_{CaO} \cdot K^{CaO}_{*S^{2-}}(P,T) + w^m_{FeO} \cdot K^{FeO}_{*S^{2-}}(P,T) + etc., \end{aligned} \quad (38)$$

where i is a melt component.

The key point about using this approach is that the dependence of volatile solubility on P, T, and melt composition can be parameterized relatively straightforwardly given sufficient experimental data on the solubility of each volatile species as a function of melt composition. However, there is no universal functional form for the solubility functions in VolFe. In some cases, they are assumed to be constant (i.e., independent of P, T, and/or melt composition); a linear combinations of oxide concentrations; or vary as functions of composition based on thermodynamic constraints or alternative empirical formulation. A variety of parameterisations for the solubility functions in terms of P, T, and X are available in the current version of VolFe. These are taken from the literature, which have been benchmarked where possible, and in a few cases we have derived new parameterizations from literature data described in the Supplementary Material (a full list of parameterisations included in VolFe is given in Tables S3–8). Additional parameterisations can be added as new experimental data and parameterisations become available for all species (an example of this is shown in the ReadTheDocs).

Of particular importance for all models of volatile solubility and degassing is the strong dependence of the solubility of CO_2 (i.e., $CO_{2,T}$) on melt composition (e.g., Blank and Brooker, 1994; Shishkina et al., 2014; Wieser et al., 2022a). Parameterisations of $CO_{2,T}$ solubility currently available in VolFe from the literature (see full list in Table S3) are each typically valid over a narrow range of

melt composition, with the range of all included parameterisations ranging from MORB through to alkali-rich compositions such as leucitite (Dixon, 1997; Dixon et al., 1995; Holloway and Blank, 1994; Lesne et al., 2011a; Thibault and Holloway, 1994), and for rhyolite (Blank et al., 1993). To then speciate $CO_{2,T}$ as $CO_{2,mol}$ and CO_3^{2-} in VolFe, current options for the equilibrium constant for eq. (20) are for basalt (all CO_3^{2-}), andesite or dacite (both CO_3^{2-} and $CO_{2,mol}$; Botcharnikov et al., 2006), and rhyolite (all $CO_{2,mol}$) (Table S4). Note that currently, the effect of H_2O on CO_2 solubility is not included (e.g., Iacono-Marziano et al., 2012b; King and Holloway, 2002; Papale et al., 2006).

The solubility function for H_2O_T is far less dependent on melt composition than $CO_{2,T}$ over the compositional range of abundant natural magmas (e.g., Allison et al., 2022; Iacono-Marziano et al., 2012; Lesne et al., 2011; Moore et al., 1998). Currently in VolFe, there are representative values for the solubility functions of basalt (Hughes et al., 2024, using data from the compilation of Allison et al., 2022) and rhyolite (derived in Supplementary Material Section S1.1 and Figure S1 using data from Blank et al., 1993; Kadik et al., 1972; Silver et al., 1990) (Table S5).

There is limited experimental data for the solubility of CO, CH_4, and H_2 in natural silicate melt compositions. Parameterisations currently available in VolFe are for H_2 in basalt and andesite (Hughes et al., 2024b, using data from Hirschmann et al., 2012); CO in basalt (Hughes et al., 2024b, using data from Armstrong et al., 2015; Stanley et al., 2014; Wetzel et al., 2013), and CH_4 in basalt (Ardia et al., 2013) (Table S8).

There is a wealth of experimental data that have been used to parameterize the solubility functions (often called capacities) for $*S^{2-}$ (Boulliung and Wood, 2023; O'Neill, 2021) and SO_4^{2-} (Boulliung and Wood, 2023a, 2023b, 2022; O'Neill and Mavrogenes, 2022), which have been included in VolFe (Table S6–7). These cover a wide range of melt compositions (basalts through rhyolite) and *T*, but not *P* (although some parameterisations include a *P* dependence). For the H_2S solubility function in VolFe, parameterisations are given in Hughes et al. (2024b) for basalt and basaltic andesite based on data from Lesne et al. (2015) and Moune et al. (2009) (Table S8).

Parameterisations for the solubility functions for inert atomic species are included in VolFe for Ar and Ne in basalt or rhyolite using data from Iacono-Marziano et al. (2010) (Supplementary Material Section S1.1, Figure S2, and Table S8). The user can also just type a numerical value to use as the solubility function (i.e., a constant) within the VolFe framework.

3.5 Treatment of f_{O2}, Fe^{3+}/Fe_T, and total oxygen content

The final linearly independent equilibrium is one that describes equilibrium between FeO and $FeO_{1.5}$. We have chosen the widely utilized, heterogeneous melt-vapor equilibrium for this purpose (e.g., Sack et al., 1981) given as eq. (21) in Table 3.

Several parameterisations for the relationship between f_{O2} and Fe^{3+}/Fe^{2+} in the melt covering a wide range of *P*, *T*, and melt composition are available in VolFe (Borisov et al., 2018; Kress and Carmichael, 1991; O'Neill et al., 2018; Table S9), which have been benchmarked where possible.

By including eq. (21), VolFe returns the values of f_{O2} and Fe^{3+}/Fe^{2+} of the equilibrium state of the system. For some calculations using VolFe, f_{O2} or Fe^{3+}/Fe^{2+} are taken as independent variables (e.g., determination of P^{v}_{sat} described in Section 4.1). In such cases, the bulk oxygen content of the system varies depending on the values of the independent variables. For other calculations (e.g., closed-system degassing described in Section 4.3), f_{O2} or Fe^{3+}/Fe^{2+} are dependent variables that vary with the path of the independent variables because the bulk O content of the system is conserved. Currently, VolFe does not include the option to externally buffer the f_{O2} (e.g., maintain the system at a given ΔFMQ during degassing) where the system is open to oxygen (e.g., CHOSETTO, Moretti et al., 2003; Moretti and Papale, 2004).

Only one f_{O2}-dependent variable (f_{O2}, Fe^{3+}/Fe_T, or S^{6+}/S_T) can be chosen as an independent variable in calculations currently implemented in VolFe. If the user specifies more than one such f_{O2}-dependent variable as independent, a warning will be raised and VolFe will alert the user to its choice of a single independent f_{O2}-dependent variable.

3.6 Sulfide, anhydrite, and graphite

Given the conditions (*P*, *T*, f_{O2}) and compositions of the melt ± vapor, VolFe can determine whether the system is supersaturated with respect to sulfide, anhydrite, and/or graphite. This is done by comparing the $*S^{2-}$ content of the melt to the sulfide content at sulfide saturation (S^{2-}CSS, eq. 39); the S^{6+} content of the melt to the sulfate content at anhydrite saturation (S^{6+}CAS, eq. 40); and the (f_{CO2}/f_{O2}) ratio of the vapor to the equilibrium constant for graphite formation (eq. 41) (Table 4). If the silicate melt is supersaturated with respect to any of these phases (i.e., eq. 39, 40, or 41 are satisfied), the calculated coexisting silicate melt and vapor compositions are metastable relative to an assemblage containing one or more of these phases. In this case, as in Hughes et al. (2022), VolFe can limit the sulfur or carbon content of the silicate melt to that at the saturation condition (i.e., satisfy the equations in Table 4). For graphite, this is equivalent to graphite precipitation, although the amount of graphite that forms is not calculated. For sulfide liquid and anhydrite, this would only approximate their precipitation because the non-volatile melt composition does not change in the VolFe calculation even though in reality it would (i.e., the FeO and CaO of the silicate melt should change) and the amount of the sulfide liquid and anhydrite phases are not calculated.

Table 4. Saturation conditions for sulfide, anhydrite, and graphite.

Phase	Saturation condition	Eq. no.

Sulfide	$S^{2-}CSS = w^{m}_{*S^{2-}}$	(39)
Anhydrite	$S^{6+}CAS = w^{m}_{S^{6+}}$	(40)
Graphite	$K_G = \frac{f_{CO_2}}{f_{O_2}}$	(41)

Notes: $S^{2-}CSS$ = sulfide content at sulfide saturation; $S^{6+}CAS$ = sulfate content at anhydrite saturation; w^{m}_{i} = weight fraction in the melt of species *i*; f_i = fugacity of species *i*; K_G = equilibrium constant for $C_G(s) + O_2(v) = CO_2(v)$.

For graphite, the parameterisation of the equilibrium constant from Holloway et al. (1992) is available in VolFe (Table S10). For the $S^{2-}CSS$, VolFe assumes the sulfide liquid phase is pure FeS unless concentrations of Fe, Cu and/or Ni in the sulfide are specified by the usert (note that not all parameterisations account for the presence of Cu or Ni). There are several different parameterisations from the literature for $S^{2-}CSS$ and $S^{6+}CAS$ available in the current version of VolFe (some of which have been benchmarked); these cover a wide range of *P*, *T*, and melt compositions for the $S^{2-}CSS$ (Fortin et al., 2015; Liu et al., 2021, 2007; O'Neill, 2021; O'Neill and Mavrogenes, 2022; Smythe et al., 2017) and $S^{6+}CAS$ (Chowdhury and Dasgupta, 2019; Zajacz and Tsay, 2019), mostly implemented using the PySulfSat Python package (Wieser and Gleeson, 2023) for their calculation (Table S10).

4 Calculation types in VolFe

Given the thermodynamic framework and model-dependent variables (Section 3), VolFe calculates the equilibrium state of the system given the choice of independent variables. As emphasized throughout, different calculation types are possible by choosing different independent variables. In the current implementation of VolFe, *T* is always one of the independent variables and is set by the user. Here we outline the three main types of calculations (e.g., Hughes et al., 2024b, 2022), as well as some additional potentially interesting calculations, currently addressable using functions built into VolFe as illustrated in Figure 2. Details of exactly how to implement the calculations and worked examples are given in the ReadTheDocs.

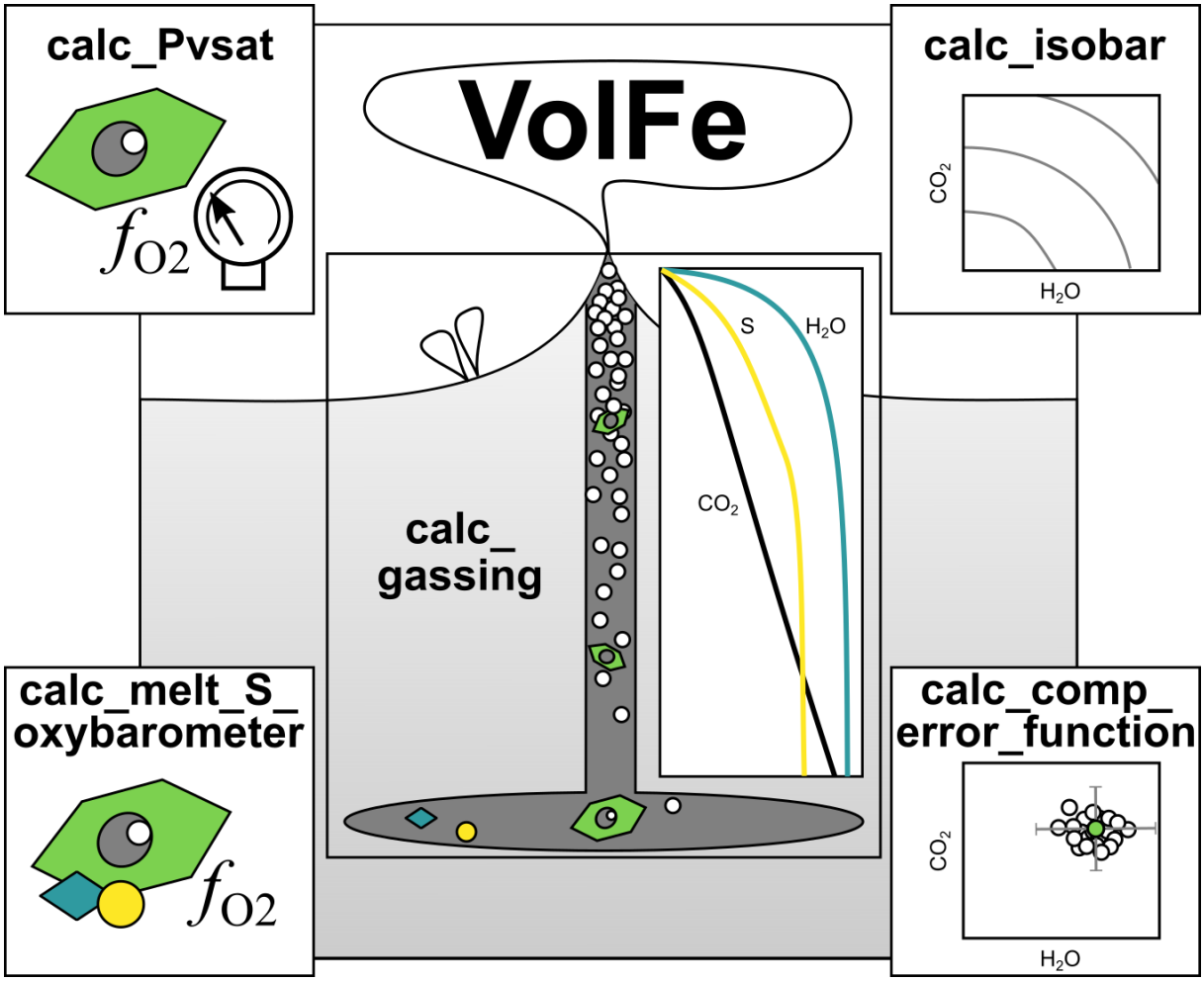

Figure 2. Schematic figure showing the key functions in VolFe: *calc_Pvsat* = calculate the pressure of vapor-saturation for a given melt composition and *T* (Section 4.1); *calc_isobar* = calculate varying H_2O-CO_2 concentrations at a given *P* and *T* (Section 4.2); *calc_gassing* = calculate isothermal open- and closed-system degassing and regassing paths (Section 4.3); *calc_melt_S_oxybarometer* = calculate the f_{O2} range for a given melt composition based on the sulfur content assuming sulfide- and anhydrite-saturation (Section 4.4); and *calc_comp_error_function* = Monte Carlo approach to generate melt compositions within analytical error and run them through *calc_Pvsat* or *calc_melt_S_oxybarometer* (Section 4.5).

The required inputs for each calculation are detailed in the following subsections. Volatile concentrations are specified as the equivalent amounts of total hydrogen as H_2O (termed H_2O-eq, wt%), total carbon as CO_2 (CO_2-eq, ppmw), and total sulfur (S_T, ppmw). The total amount of the "X" component is simply referred to as "X" (ppmw) since there is only a single melt and vapor "X"-bearing species. For the calculations, the volatile contents (i.e., the absolute values of H_2O-eq, CO_2-eq, S, and "X") are used directly as inputted, whilst the volatile-free melt composition (SiO_2, TiO_2, etc.) is recalculated such that is sums to 100 wt% minus the sum of the total volatiles (example in Table S12).

We illustrate the use of VolFe in understanding natural systems by applying the calculations described in this section to data from the Marianas arc (Brounce et al., 2014; Kelley and Cottrell, 2012), using the Fe^{3+}/Fe_T values from Cottrell et al. (2021) where available that have been recalculated using the updated Mössbauer-XANES calibration of Zhang et al. (2018). These data were chosen because they have CO_2-eq, H_2O-eq, S, Fe^{3+}/Fe_T, and major element composition measured for each olivine-hosted basaltic melt inclusion glass (MI, n = 49; Arigan = circle, Sarigan = triangle, and Alamagan = square) and basaltic-andesite submarine pillow glass (SPG, n = 2; Southern Mariana Trough = diamond), which are required inputs for most VolFe calculations (e.g., measured composition in Figure 3). See Table S13 for species and model dependent variables used in the calculations. We recommend that the original reference for the specific parameterisations of the model-dependent variables used within the VolFe calculations be clearly cited. Additionally, if the parameterisation is implemented in VolFe using an external Python package this should also be cited (e.g., S^{2-}CSS using PySulfSat by Wieser and Gleeson, 2023; melt density using DensityX by Iacovino and Till, 2018). The T chosen for each glass composition was calculated based on the measured volatile-free melt composition and H_2O-eq using eq. (14) from Putirka (2008) as implemented in Thermobar (v1.0.41; Wieser et al., 2022) (Figure 4a). These calculated T (Figure 4a) were then used in the VolFe calculations presented here, all of which used VolFe v0.4.1. A Jupyter notebook for this full workflow is on the GitHub and ReadTheDocs and can be used as a template for data processing.

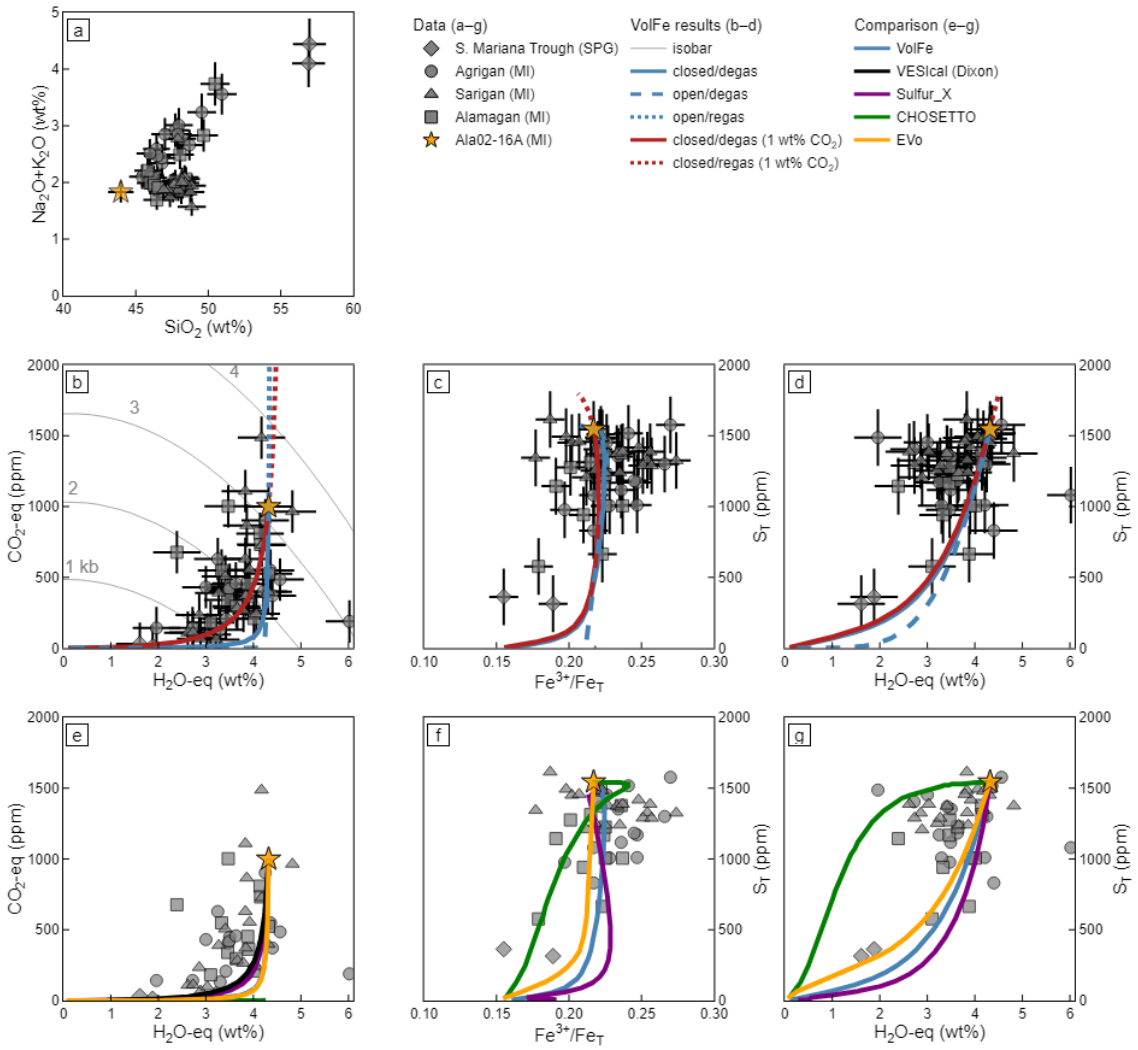

Figure 3. Measured melt inclusion (MI) and submarine pillow glass (SPG) data from the Marianas arc (Brounce et al., 2014; Kelley and Cottrell, 2012; Cottrell et al., 2021) and modelling results using VolFe and some other available tools: **(a)** normalised SiO_2 vs. normalised total alkalis (Na_2O+K_2O); **(b,e)** CO_2-eq vs. H_2O-eq; **(c,f)** S_T vs. Fe^{3+}/Fe_T; and **(d,g)** S_T vs. H_2O-eq. Symbols are measured data (grey), where the shape indicates MI or SPG and volcano with 2 sigma errors bars (diamond = Southern Mariana Trough SPG, circle = Agrigan MI, square = Sarigan MI, triangle = Alamagan MI, and yellow star = Ala02-16A MI). Isobars (grey curves) are shown in (b) for Ala02-16A. Re- and degassing paths are shown in (b–d) starting from the composition of Ala02-16A assuming: closed-system degassing (blue solid); closed-system degassing (red solid) and regassing (red dot) with 1 wt% initial CO_2; and open-system degassing (blue dash) and regassing (blue dot). The closed-system degassing calculation where the MI Ala02-16A represents the bulk composition (i.e., the solid blue curve in b–d) for VolFe (blue: under the orange-Evo curve in e), VESIcal

(Dixon, black – e only), Sulfur_X (purple), CHOSETTO (green: essentially along the x-axis in e), and Evo (orange) are shown in e–g (error bars are omitted in these panels for clarity).

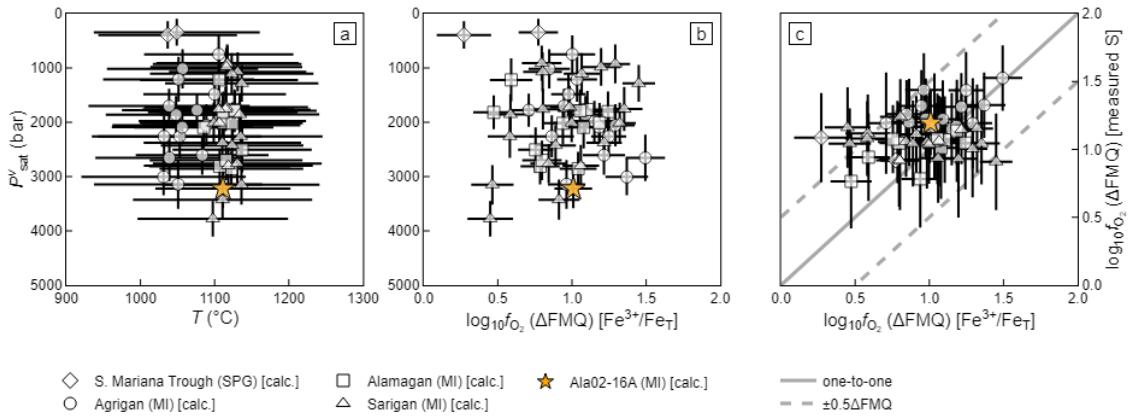

Figure 4. Results for the pressure of vapor-saturation barometer calculations using measured Fe^{3+}/Fe_T (Section 4.1) for the Marianas dataset showing calculated P^v_{sat} vs. **(a)** calculate T using eq. (14) from Putirka (2008) implemented in Thermobar (Wieser et al., 2022b); and **(b)** calculated ΔFMQ from Fe^{3+}/Fe_T. **(c)** Calculated ΔFMQ using measured sulfur concentration vs. calculated ΔFMQ using measured Fe^{3+}/Fe_T, where the solid line is the one-to-one relationship and dotted lines are ±0.5ΔFMQ. Symbol shape indicates MI or SPG and volcano (diamond = Southern Mariana Trough SPG, circle = Agrigan MI, square = Sarigan MI, triangle = Alamagan MI, and yellow star = Ala02-16A MI), which are white as all values are calculated rather than measured. Associated error bars are 2 sigma values based on calculations using 100 compositions generated from a Monte Carlo approach (see text for details).

4.1 The pressure of vapor-saturation of a magma and its use as a geobarometer

The dissolved volatile contents of a melt in equilibrium with a vapor can be used as a barometer because the sum of the partial pressures of all the vapor species (P^v_{sat}) must equal the total pressure (eq. 10) (e.g., Anderson et al., 1989; Blundy and Cashman, 2008; Hughes et al., 2024). Calculations of P^v_{sat} have been widely applied to melt inclusions to calculate magma storage depths (e.g., Black and Andrews, 2020; Camejo-Harry et al., 2019, 2018; Colman et al., 2015; Wanless et al., 2015; Wieser et al., 2021) and to sub-aqueous matrix glasses to calculate eruption depths (e.g., Belgrano et al., 2021; Coombs et al., 2006; Lund et al., 2018; Seaman et al., 2004). As the phase proportions are not required, the phase rule defines the number of independent variables required (eq. 2: F = 2–5 depending on the number of volatile species in the system). The independent variables used in VolFe for this calculation are T; the total concentrations of C, H, S, and/or "X" in the melt (depending on which volatiles are present in the system); and an f_{O2}-dependent variable (e.g., f_{O2}, Fe^{3+}/Fe_T, or S^{6+}/S_T). From this, P^v_{sat}, the melt speciation (i.e., concentrations of the various dissolved melt species), and the vapor composition and speciation are calculated. This calculation is outlined in detail in Hughes et al.

(2024b) (Figure 5). In brief, the pressure and melt speciation are iteratively calculated until the sum of the partial pressures of all the vapor species equals the total pressure (i.e., eq. 10 is satisfied).

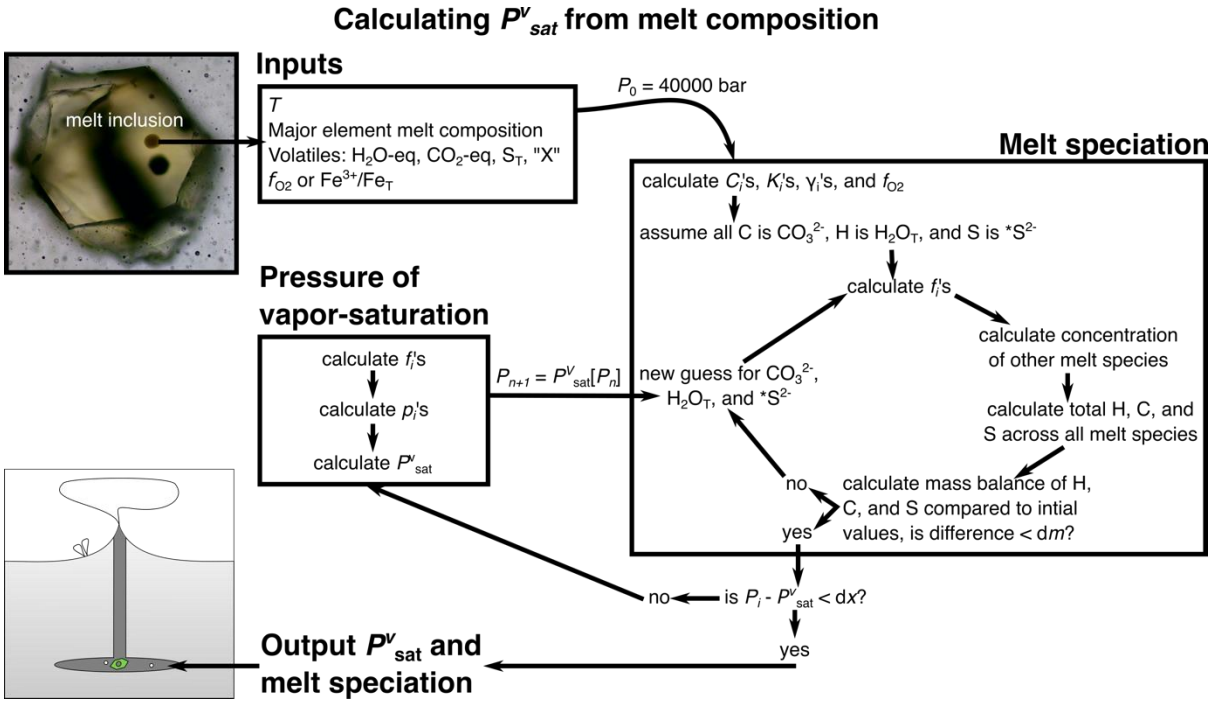

Figure 5. Flow chart describing the calculation of the pressure of vapor-saturation. Adapted from the Supplementary Material of Hughes et al. (2024b). *Abbreviations:* P^v_{sat} = pressure of vapor saturation; T = temperature; H_2O-eq = equivalent amount of H as H_2O; CO_2-eq = equivalent amount of C as CO_2; S_T = total sulfur; P_0 = initial P guess; P_n = P at iteration n; C = solubility function; K = equilibrium constant; γ = fugacity coefficient; f = fugacity; p = partial pressure; dm = mass balance tolerance; and dx = P tolerance.

As an example, P^v_{sat} and f_{O2} were calculated for each glass composition from the Marianas dataset (Figure 4a–b). Note that these studies only measured the CO_2 content of the glass within the melt inclusion and did not measure the CO_2 content of any coexisting vapor bubbles (Brounce et al., 2014; Cottrell and Kelley, 2012). This means the total CO_2 content of the melt inclusions is likely underestimated, which means entrapment pressures of the melt inclusions will be underestimated if assumed to equal P^v_{sat} (Wieser et al. 2021; Wallace et al., 2015; Moore et al., 2015; Hartley et al., 2014). Hence, more accurate entrapment pressures using P^v_{sat} will be calculated from melt inclusion data where CO_2 in both the glass and bubble is measured and combined to calculate the melt content at entrapment.

4.2 Isobars

Vapor-saturated isobars are curves or surfaces of vapor-saturated melt compositions for a fixed volatile-free base melt composition at a given P^v_{sat}. Typically, they are shown as the loci of pairs of experimentally-determined or model-calculated concentrations of H_2O_T and $CO_{2,T}$ in vapor-saturated

melt at a single P (and T) but spanning $H_2O_T/(H_2O_T + CO_{2,T})$ from 0 to 1 in the vapor. Such diagrams have been widely used to compare the H_2O_T and $CO_{2,T}$ concentrations on these isobars to measured values in melt inclusions and matrix glasses to estimate P^v_{sat} at entrapment for melt inclusions and eruption for the matrix glasses (e.g., Dixon & Stolper, 1995). Such determinations are subject to a variety of caveats (e.g., Wieser et al., 2022a).

VolFe can be used to calculate such isobars at a given T and volatile-free melt composition assuming the melt only contains H_2O_T and $CO_{2,T}$ and the vapor only contains H_2O and CO_2. For each P, first VolFe calculates the $CO_{2,T}$ content of the melt with no H_2O_T present and the concentration of H_2O_T in the melt with no $CO_{2,T}$ present. Next, at 20 equal intervals of H_2O_T concentration in the melt between 0 and the maximum H_2O_T, VolFe calculates the associated p_{H2O}. Then, p_{CO2} is calculated from $(P - p_{H2O})$, and finally the $CO_{2,T}$ concentration in the melt is calculated. As an example, we used the composition of Ala02-16A (i.e., measured volatile-free melt composition and calculated T; Fe^{3+}/Fe_T and S are not included in this calculation) to calculate isobars for varying H_2O_T and $CO_{2,T}$ at 1000–4000 bar in 1000 bar increments (Figure 3b). Additionally, a comparison to isobars calculated using the Dixon (1997) model in VESIcal (Iacovino et al., 2021) are shown in Figure S4.

4.3 Degassing and regassing paths

The main application we envision for VolFe is calculation of the compositions (including Fe^{3+}/Fe_T and therefore f_{O2}) and mass fractions of coexisting melt and vapor during magma degassing. For these calculations, the bulk composition of the system is specified, and P and T are the independent variables. Currently, VolFe only considers isothermal paths of vapor-saturated melt (i.e., varying P at constant T), which could be adapted in the future. We refer to paths of decreasing P where vapor-saturated melt ascends as "degassing", resulting in progressive exsolution of volatiles from melt into vapor. The reverse occurs (i.e., progressive dissolution into the melt of volatiles in the vapor) with increasing P; we refer to this as "regassing". Regassing can happen in nature when subaerial, vesicular lava flows enter the ocean causing bubble resorption (e.g., Moore et al., 1985) or in downward limbs of a convecting bubbly magma chambers and conduits (e.g., Carey et al., 2013). The concept of regassing can also be used to reconstruct the undegassed (or less degassed) volatile contents of parental magmas. VolFe also allows the bulk composition of the system to be varied in successive steps (e.g., by removal or by addition of the vapor in equilibrium with melt at each step) to simulate open-system behaviour. Melt density is calculated using DensityX (Iacovino and Till, 2018) in VolFe along these P-T paths.

The exact way in which the equations are solved for these processes by VolFe depends on the number of vapor species assumed to be present but is the same for closed- and open-system regassing and degassing calculations. Here, we describe briefly the calculations for a magma containing COHS-bearing volatile species (i.e., all ten vapor species, except "X"; Figure 6). Each step is solved for a given

bulk composition of the system at fixed values of P and T. Given reasonable starting guesses for the mole fractions of three independent vapor species (e.g., O_2, CO, and S_2), the concentrations of all other melt and vapor species can be calculated iteratively from the homogeneous vapor and heterogeneous melt-vapor equilibria in eq. (3–8) and (11–19). Using these calculated vapor concentrations and the mass balances for C, H, O, and S across melt and vapor, we calculate the weight fraction of vapor based on each volatile element (eq. 22–33). The "solver" currently uses the Jacobian matrix/Newton-Raphson approach and the differential equations were generated using SymPy (Meurer et al., 2017) from the equations in Section 3.3. The values for the mole fractions of the "guessed" vapor species are then updated in successive iterations until the difference in estimates of vapor weight fraction from each volatile element are within a specified tolerance (typically 10^{-9} weight fraction). The mole fraction of O_2 is always one of the "guessed" species to ensure numerical convergence as it has a small absolute value and would be difficult to calculate subsequently via mass balance (further discussion in Supplementary Material Section S3). Crucial to this approach is good initial guesses of the three vapor mole fractions at each P-step. We use values from the previous calculation step as initial guesses, which is particularly useful at the start of the degassing calculation as we can use the values at P^{v}_{sat} as starting guesses for the first P-step. Currently, the initial P that VolFe starts re- and degassing calculations is always the P^{v}_{sat} of the given melt composition (i.e., the user cannot specify the initial P). Further details of our approach are provided in Supplementary Material Section S3.

Note that this specific calculation in VolFe requires using the relationship between f_{O2} and Fe^{3+}/Fe^{2+} from eq. (A-5,6) in Kress and Carmichael (1991) (i.e., the other parameterisations in Table S9 cannot be used currently). Equations (A-5,6) were chosen due to their thermodynamic formulation rather than the empirical form of the more widely used eq. (7) from Kress and Carmichael (1991). Results using eq. (A-5,6) are expected to be similar to those using eq. (7) because Kress and Carmichael (1991) report that both reproduce the input experimental data equally well (standard errors of 0.33 and 0.37 wt% for FeO and Fe_2O_3, respectively, for eq. A-5,6 compared to 0.21 and 0.42 wt% for eq. 7) and results using both equations are essentially indistinguishable in Figure 3 of Kress and Carmichael (1991).

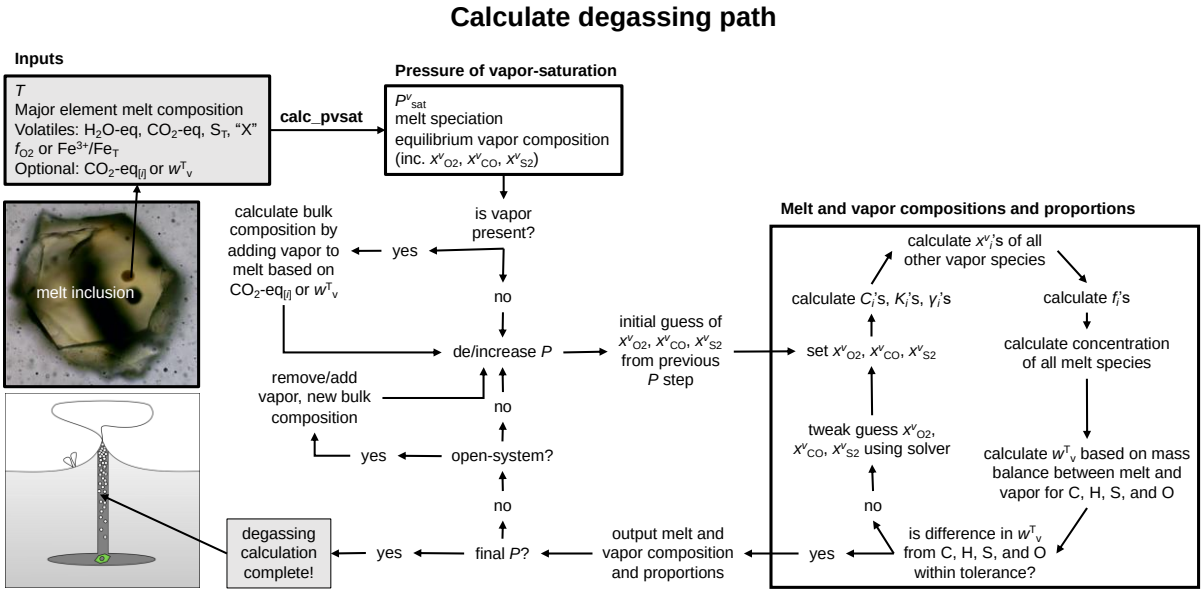

Figure 6. Flow chart describing the re/degassing calculation. *Abbreviations:* P^{v}_{sat} = pressure of vapor-saturation; P = pressure; T = temperature; H_2O-eq = equivalent amount of H as H_2O; CO_2-eq = equivalent amount of C as CO_2; S_T = total sulfur; CO_2-eq$_{[i]}$ = bulk CO_2-eq concentration of the system if different to CO_2-eq; w^{T}_{v} = weight fraction of the vapor; x^{v}_{i} = mole fraction in the vapor; C = solubility function; K = equilibrium constant; γ = fugacity coefficient; and f = fugacity.

For closed-system calculations, the bulk composition of the system remains constant (i.e., the bulk concentrations of C, O, S, H, "X", and silicate component); the evolving melt and vapor remain in chemical equilibrium throughout; and regassing is simply the reverse of degassing. For open-system degassing, the vapor is removed at each *P*-step and the melt composition becomes the bulk composition of the system for the next step. For open-system regassing, a small increment of vapor that is in equilibrium with the melt is added to the system defining a new bulk composition (the amount of vapor can be user-defined). This procedure can be calculated *ad infinitum*, but in practice it would be stopped at some point defined by constraints external to the VolFe calculations (e.g., at a particular *P*, CO_2, H_2O, etc. content believed reasonable based on other petrological arguments: currently it stops at a user-defined *P*). This open-system regassing calculation is precisely analogous to correcting for fractional crystallization of olivine from a parental melt for an evolved basalt that only has olivine on its low-*P* liquidus. Hence, open-system regassing can be used to reconstruct the initial composition of a parental or even primary melt.

Both open- and closed-system regassing and degassing calculations in VolFe require a *T* and an initial melt composition (i.e., the volatile-free melt composition, CO_2-eq, H_2O-eq, S_T and/or "X", and f_{O2} value or measured Fe^{3+}/Fe_T or S^{6+}/S_T) from which to start the calculation. For a glassy pillow rim from the sea floor, the required melt composition could simply be taken as the measured glass composition. For a melt inclusion, the required melt composition could be the bulk composition of the melt inclusion at the time of entrapment (i.e., correcting for vapor bubble formation, post-entrapment

crystallisation, etc.; e.g., Rose-Koga et al., 2021). Regardless of how it is obtained, this melt composition fixes the bulk composition of the system if there is no vapor present. This is always the starting condition for open-system regassing and degassing calculations and can be the starting condition for closed-system degassing calculations.

Alternatively, the melt composition at the start of the calculation might coexist with a vapor (e.g., in an ascending magma in which degassing had already begun). Coexisting melt and vapor must be the starting condition for closed-system regassing and could be the starting condition for closed-system degassing. If the amount of coexisting vapor prior to increasing or decreasing P is known or estimated, this can be specified as in input in VolFe: VolFe then calculates the composition of this equilibrium vapor at P^{v}_{sat} given the specified melt composition (e.g., Section 4.1). The bulk composition of the system is then calculated as the weighted combination of the compositions of coexisting melt and vapor and the starting point for the calculation is a melt+vapor assemblage. However, the amount of vapor is often unknown. In such cases, it might be possible to estimate the bulk CO_2 content of the undegassed magma (e.g., Macpherson and Mattey, 1994; Moore and Bodnar, 2019). The amount of vapor present can then be calculated given mass balance between the carbon in the melt and vapor at P^{v}_{sat} (the composition of the melt is known and the composition of the vapor is calculated as in Section 4.1) and the initial carbon (eq. 22–25). From this, the initial composition of all volatiles can be calculated and therefore the bulk composition of the system specified.

For closed-system calculations, the bulk composition of the system (including O) is fixed. The constancy of total O results in systematic variations in all dependent variables with progressive re- and degassing, because f_{O2}, Fe^{3+}/Fe_T and S^{6+}/S_T are all dependent variables. For VolFe, open-system does not mean the system is open only to O, as would be the case if f_{O2} were fixed (e.g., buffered) externally. As with closed-system calculations, the changing composition of the system at each step during open-system calculations results in continuous variations in f_{O2} and Fe^{3+}/Fe_T and S^{6+}/S_T because these are dependent variables.

At each P-step for open- or closed-system regassing or degassing, the calculated equilibrium melt composition is checked for saturation with respect to graphite, liquid sulfide, and/or anhydrite (see section 3.6). If the melt composition is supersaturated with respect to one or more of these phases, the user can specify that the carbon and/or sulfur content of the melt is capped at the value of saturation (e.g., the $*S^{2-}$ content of the melt is equal to S^{2-}CSS; Section 3.6) and the equilibrium state of the system is found at this capped sulfur and/or carbon content. However, the major element composition of the melt does not change to account for sulfide and/or anhdyrite formation (i.e., Fe and Ca do not change). In this case, the "excess" S and/or C from the previous step (e.g., for sulfide supersaturation, this is the difference in $*S^{2-}$ between the metastable supersaturated melt $*S^{2-}$ content and that of sulfide-saturated melt for the same base melt composition) is sequestered for consideration in the next P-step. For open-system calculations, the additional C and/or S are then removed from the system for the next P-step. For closed-system calculations, if the S and/or C content of the melt drops below graphite, liquid sulfide,

and/or anhydrite saturation at a subsequent *P*, the sequestered C and/or S are added back to the system. This treatment of supersaturation is crude and involves a variety of approximations. However, given the small amounts of sulfide and/or anhydrite that are likely to precipitate for natural systems, and therefore the small change in major element melt composition, we feel this simplified treatment is likely to give reasonable results.

As an example, we calculated various closed- and open-system regassing and degassing paths with Ala02-16A as the starting melt composition i.e., measured glass composition has 999 ppm CO_2-eq, 4.52 wt% H_2O-eq, 1544 S_T, and 0.238 Fe^{3+}/Fe_T, volatile-free melt composition, and the calculated *T* is 1111 °C): (1) isothermal closed-system degassing with no vapor present at the start of degassing; (2) isothermal open-system degassing; (3) isothermal open-system regassing; and isothermal closed-system (4) degassing and (5) regassing where the bulk system contains 1 wt% CO_2 (i.e., vapor is present at the yellow star) (Figure 3b–d). Regassing calculations went up to 5000 bar and could be used to estimate the composition and P^v_{sat} of permissible parental liquids from which the entrapped melt inclusion glasses formed by degassing. For comparison to the degassing paths, we plot the measured (grey symbols: CO_2-eq, H_2O-eq, S_T, and Fe^{3+}/Fe_T) or calculated at P^v_{sat} (white symbols: S^{6+}/S_T, ΔFMQ, and vapor composition) values for the individual melt inclusion and submarine pillow glass analyses (Figure 3, Figure 7, and Figure 8). However, the glasses come from different volcanoes and are therefore not related by simple re- and degassing processes (Brounce et al., 2014; Kelley and Cottrell, 2012) and melt composition and *T* are not constant for the melt inclusion and submarine pillow glass data but are for the calculated re- and degassing paths.

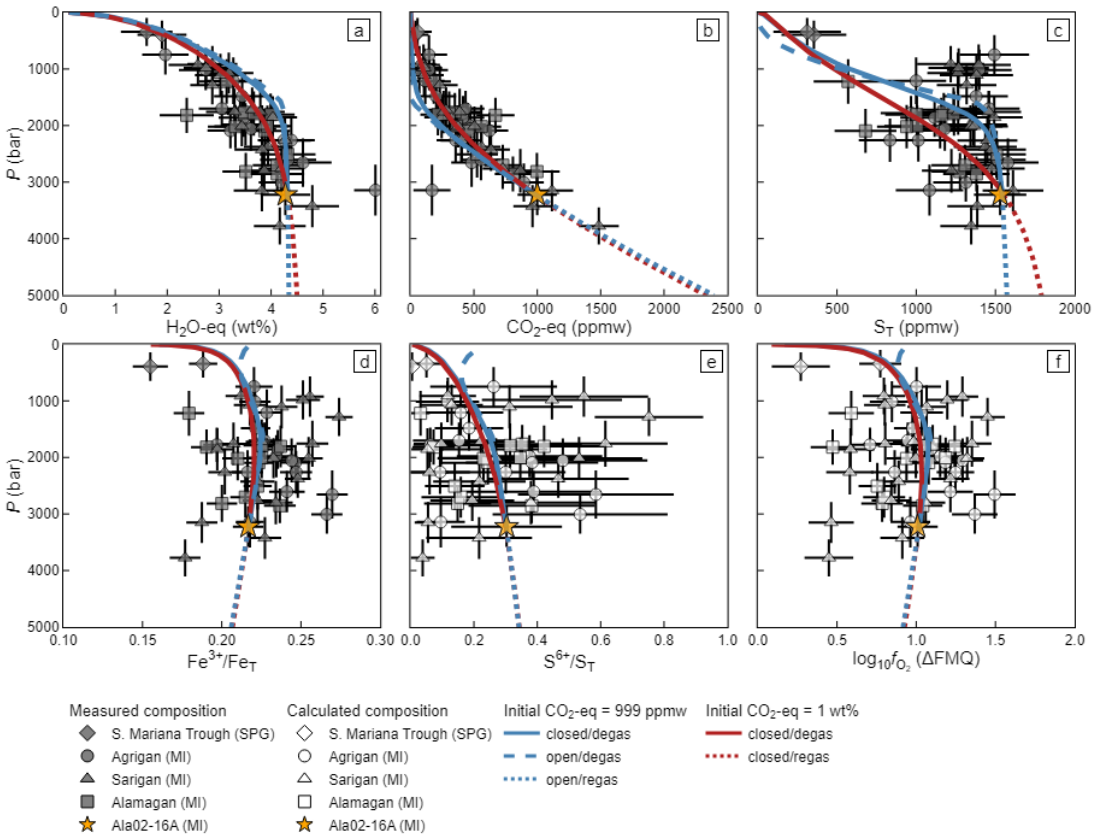

688

689 Figure 7. Melt composition for open- and closed-system re- and degassing calculations (Section 4.3) for
690 Ala02-16A from the Marianas dataset, showing *P* vs. **(a)** H_2O-eq, **(b)** CO_2-eq, **(c)** S_T, **(d)** Fe^{3+}/Fe_T; **(e)** S^{6+}/S_T,
691 and **(f)** ΔFMQ. Curves begin at melt inclusion Ala02-16A (yellow star) for: closed-system degassing
692 assuming Ala02-16A represents the bulk composition of the system (blue solid); closed-system degassing
693 (red solid) and regassing (red dot) assuming the bulk system contains 1 wt% CO_2-eq; and open-system
694 degassing (blue dash) and regassing (blue dot). Symbols show measured melt volatile contents (grey, a–d)
695 or calculated values (white, e and f) at calculated P^v_{sat} (Section 4.1) for natural glasses for comparison with
696 the degassing paths calculated using VolFe. The shape indicates MI or SPG and volcano (diamond =
697 Southern Mariana Trough SPG, circle = Agrigan MI, square = Sarigan MI, and triangle = Alamagan MI).

Error bars are 2 sigma based on measurement uncertainty or propagated uncertainty using a Monte Carlo approach.

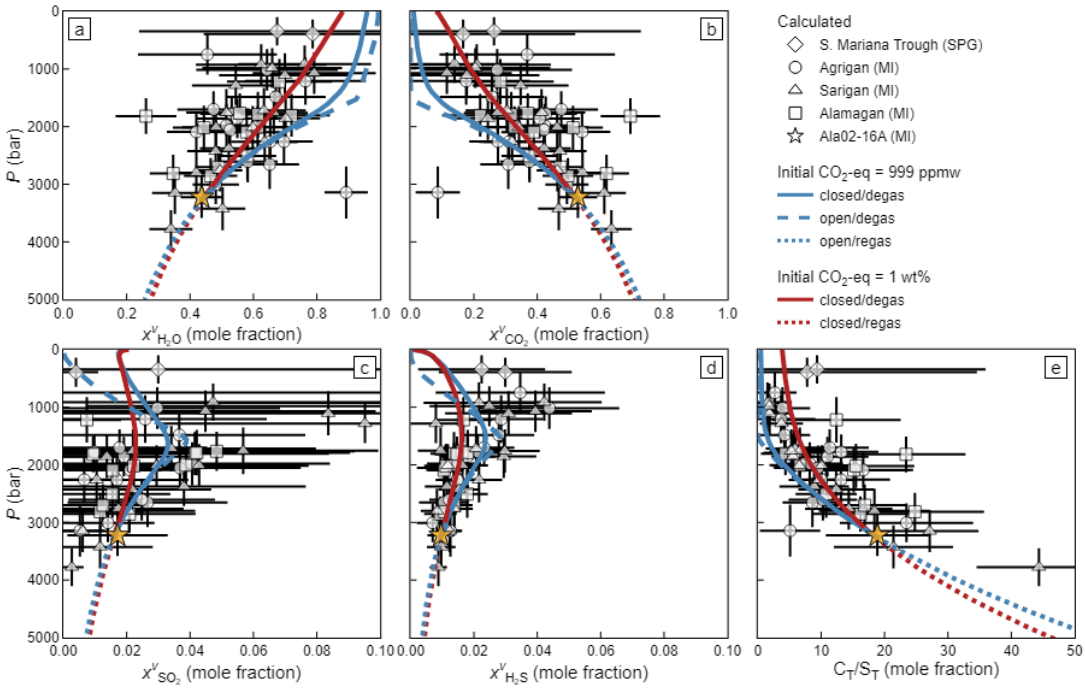

Figure 8. Vapor composition for open- and closed-system re- and degassing calculations (Section 4.3) for Ala02-16A from the Marianas dataset, showing *P* vs. mole fraction in the vapor for: **(a)** H_2O, **(b)** CO_2, **(c)** SO_2, **(d)** H_2S; and **(e)** C_T/S_T. All other vapor species (O_2, H_2, CO, S_2, CH_4, and OCS) are always <0.01 mole fraction. Curves begin at melt inclusion Ala02-16A (yellow star) for: closed-system degassing assuming Ala02-16A represents the bulk composition of the system (blue solid); closed-system degassing (red solid) and regassing (red dot) assuming the bulk system has 1 wt% CO_2-eq; and open-system degassing (blue dash) and regassing (blue dot). Symbols (white) show calculated vapor speciation at calculated P^v_{sat} (Section 4.1) for natural glasses for comparison with the degassing paths calculated using VolFe. The shape indicates MI or SPG and volcano (diamond = Southern Mariana Trough SPG, circle = Agrigan MI, square = Sarigan MI, and triangle = Alamagan MI). Error bars are 2 sigma based on propagated uncertainty using a Monte Carlo approach.

4.4 The "total melt sulfur oxybarometer" based on the sulfur contents of melts and glasses

Oxygen fugacity is a key thermodynamic parameter in magmatic systems because of its effects on the chemical and physical properties of the melt, the crystallization sequence and liquid line of descent, the speciation of magmatic gases, etc. (e.g., Carmichael and Ghiorso, 1990; Hughes et al., 2024b; Kolzenburg et al., 2018). There are many different oxybarometers available and, in certain

circumstances, the sulfur content of the melt can be used to place bounds on the f_{O2} based on sulfide liquid or anhydrite saturation (e.g., Beermann et al., 2011; Hughes et al., 2022; Muth and Wallace, 2022), using an approach that we term the "total melt sulfur oxybarometer". A short description of its implementation is given here (Figure 9); see Section "Using w^m_{ST} as an oxybarometer" in Hughes et al. (2022) for a more detailed description.

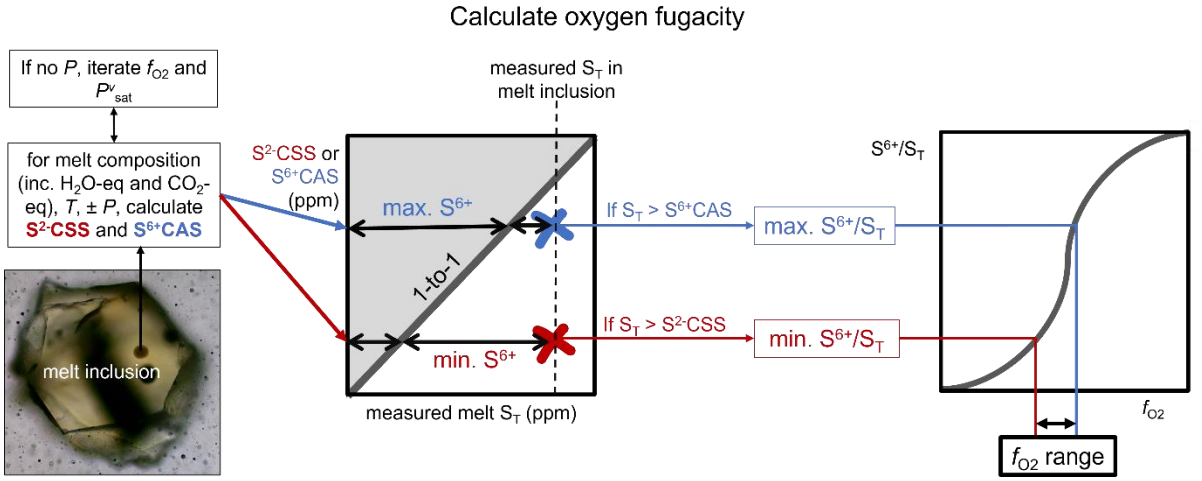

Figure 9. Schematic of how the melt sulfur content oxybarometer works. The crosses represent the measured S_T vs. calculated S^{2-}CSS and S^{6+}CAS.

In VolFe, this constraint on f_{O2} is implemented by calculating the S^{2-}CSS and S^{6+}CAS for the given conditions (T, P, and melt composition including volatiles). VolFe then compares the calculated S^{2-}CSS to the measured sulfur content (S_T). If $S_T > S^{2-}$CSS, it calculates $S^{6+}/S_T = (S_T - S^{2-}\text{CSS})/S_T$ and then converts it to f_{O2}. If $S_T < S^{2-}$CSS, it cannot calculate a minimum f_{O2}. A similar comparison is then done for the S^{6+}CAS: if $S^{6+}\text{CAS} > S_T$, a maximum f_{O2} can be calculated from $S^{6+}/S_T = S^{6+}\text{CAS}/S_T$ (no maximum f_{O2} can be calculated if $S^{6+}\text{CAS} < S_T$). If the calculation is at P^v_{sat} (rather than a specified P), VolFe iteratively calculates P and f_{O2} until convergence (note that if the specified P is too low for the given volatile content, the melt will be vapor-supersaturated and hence metastable). Hence, if the sulfur content is high enough, for a given T, volatile-free melt composition, and volatile content, a range of allowable f_{O2} values can be calculated using VolFe (Figure 9).

As an example, the measured S_T content was also used to calculate f_{O2} based on the total-melt-sulfur-oxybarometer assuming vapor-saturation for the Marianas dataset (Figure 4c). Only minimum estimates of f_{O2} were possible using the measured sulfur content because the sulfur contents were not high enough to be potentially saturated with anhydrite. A few glasses did not have sufficient sulfur for a minimum f_{O2} estimate because their sulfur contents are less than S^{2-}CSS (e.g., the two submarine pillow glasses – diamonds – are not shown in Figure 4**Error! Reference source not found.**c).

4.5 Monte Carlo errors for melt composition

Inputs to all these calculations (e.g., oxide concentration, volatile contents, Fe^{3+}/Fe_T, etc.) will have uncertainties associated with them and it can be useful to see how these errors influence the results. A Monte Carlo approach can be applied in VolFe to the measured melt composition (and T) assuming absolute or relative errors are independent from each other and normally distributed about a specified mean and standard deviation. These compositions can then be used as starting conditions for the pressure of vapor-saturation and f_{O2} from S calculations. While allowing propagation of uncertainty based on user inputs, this approach does not constrain uncertainties introduced by model-dependent variables in VolFe (e.g., solubility functions, fugacity coefficients, etc.).

To evaluate the influence of errors associated with measurements of the melt composition on calculated T, P^v_{sat}, and f_{O2}, we randomly generated 100 different compositions using this Monte Carlo approach for each melt inclusion and submarine pillow glass (Figure 3a–d). Errors were assumed to be independent and normally distributed with the following one sigma values typical for these types of analyses: ±0.25 wt% H_2O; ±75 ppm CO_2; ±100 ppm S; ±0.005 Fe^{3+}/Fe_T; ±1% relative for major oxides; ±5% relative for minor oxides, ±51 °C (standard estimate of error of this thermometer: Putirka, 2008) (note that ±2 sigma errors are shown on Figure 3a–d for all species). Each of these 100 compositions was then used to calculate P^v_{sat} and f_{O2} (but not degassing paths) as described in Sections 4.1 and 4.4 (Figure 4). Including analytical uncertainties from melt composition represents *minimum* uncertainties and does not include model error.

5 Comparison to other approaches

As emphasized in Section 1, there are several other tools available to calculate melt-vapor chemical equilibria. These tools differ from VolFe in a variety of ways, including: the volatile components considered; the melt and vapor species considered; their approach to formulation; parameterisations of model-dependent variables available; and the types of calculations for which they are best suited. A full comparison of the various tools is beyond the scope of this paper (further discussion in Supplementary Material Section S4), so only key features are discussed here; a preliminary comparison between VolFe and others tools can also be found in Hughes et al. (2023) .

The tools we compare to here are VolatileCalc (Newman and Lowenstern, 2002), VESIcal (Iacovino et al., 2021), Solcwad (Papale et al., 2006), MagmaSat (Ghiorso and Gualda, 2015), SolEx (Witham et al., 2012), Sulfur_X (Ding et al., 2023), CHOSETTO (Moretti et al., 2003; Moretti and Papale, 2004), MELTS (Ghiorso et al., 2023), Petrolog4, DCompress (Burgisser et al., 2015), Evo (Liggins et al., 2022, 2020), and MAGEC (Sun and Lee, 2022; Sun and Yao, 2024). The key similarities and differences are outlined in Table 5 and the following bullet points.

Table 5. Some of the key similarities and differences between tools available to calculate melt-vapor chemical equilibria.

	VolatileCalc	VESIcal	Solcwad	MagmaSat	SolEx	Sulfur_X	CHOSETTO	MELTS	Petrolog4	DCompress	EVo	MAGEC	VolFe
Water and CO_2 in the melt and vapor	✓	✓	✓	✓	✓	✓	✓	✓	✓	✓	✓	✓	✓
H_2, CO, and CH_4 in the melt and vapor	✗	✗	✗	✗	✗	✗	✗	✗	✗	✓	✓	✓	✓
Sulfur-bearing species in the vapor	✗	✗	✗	✗	S_T	H_2S SO_2	H_2S SO_2	H_2S SO_2	H_2S SO_2	S_2 H_2S SO_2 *	S_2 H_2S SO_2	S_2 H_2S SO_2 OCS	S_2 H_2S SO_2 OCS
Sulfur-bearing species in the melt	✗	✗	✗	✗	S_T	S^{2-} S^{6+}	S^{2-} S^{6+}	S^{2-} S^{6+}	S^{2-} S^{6+}	H_2S SO_2	S^{2-} S^{6+}	S^{2-} S^{6+}	*S^{2-} H_2S S^{6+}
Other species	✗	✗	✗	✗	Cl	✗	✗	Cl F	✗	✗	N_2	✗	"X"

Notes: * DCompress additionally considers OCS for gas species calculations at atmospheric pressure.

- Modelling sulfur: SolEx, Sulfur_X, and Petrolog4 use a partition coefficient approach rather than the solubility function approach on which DCompress, CHOSETTO, Evo, MAGEC, and VolFe are based.
- Oxygen: Sulfur_X, DCompress, Petrolog4, Evo, MAGEC, and VolFe are a closed system with respect to oxygen during closed-system degassing. CHOSETTO externally buffers the system during degassing and hence oxygen is not conserved.
- Calculation types: All these tools calculate closed-system degassing paths. Some tools calculate open-system degassing (e.g., VolatileCalc). Only VolFe calculated open- and closed regassing. Most of the tools can calculate P^{v}_{sat} (except CHOSETTO and DCompress). Some tools can calculate isobars (e.g., VolatileCalc, VESIcal, etc.). None aim to calculate melt-vapor composition for other independent variables (e.g., f_{O2} from sulfur content), although MiMIC (Rasmussen et al., 2020) can do calculations along constant volume paths based on VolatileCalc and Petrolog4 has T as a dependent variable.
- Model-dependent variables: A wide variety of parameterisations for model-dependent variables are employed across the range of tools, especially in their chosen functional forms and parameterizations of the solubility functions employed.

Overall, VolFe is most similar to Evo and MAGEC in terms of the species and reactions considered in the melt and vapor, but different parameterisations of model-dependent variables are

available in the different tools. Results of closed-system degassing calculations assuming Ala02-16A represents the bulk composition of the system using VESIcal (Dixon model), CHOSETTO, Sulfur_X, and Evo are shown in Figure 3e–f (inputs for these calculations can be found in the GitHub). As observed by Ding et al. (2023) and Hughes et al. (2024), these models produce different results due to a combination of the melt and vapor species considered, approach to formulation, and parameterisations of model-dependent variables used.

6 Future work

Our goal is to make VolFe a flexible and adaptable tool for predicting and understanding trends relating to melt-vapor equilibrium in natural magmas based on a thermodynamically consistent framework. However, the data underlying VolFe is a moving target. As we have tried to emphasize, an important feature is the ability to update VolFe by modifying it so as to include new thermochemical data (e.g., data on solubilities of various volatiles; fugacities and mixing relations of vapor species; etc.) and adding new user options (including other choices of independent variables and the paths they follow). Additionally, new calculation types can be incorporated as they become useful, as well as modifying the thermodynamic framework (e.g., new volatiles, species, phases) to enable more complex systems to be modelled. Continued improvement of interoperability with other relevant Python packages (e.g., PySulfSat, Wieser and Gleeson, 2023; DensityX, Iacovino and Till, 2018) is key to the continued improvement of geochemical modelling, as well as the evaluation and incorporation of uncertainties of model-dependent variables into calculations. A robust comparison with other melt-vapor chemical equilibria will also be crucial in enabling the community to understand the strengths and limitations of the different tools available.

7 Summary

We have described the thermodynamic framework and currently available calculation types for VolFe, an open-source Python package to calculate melt-vapor equilibria. VolFe considers a variety of both oxidised and reduced volatile-bearing species containing C, H, S, O, and noble gases such that it can be applied to terrestrial (e.g., MORB, arc, and ocean islands) and extra-terrestrial (e.g., Moon, Mars, and Io) systems. Various parameterisations of model dependent variables (e.g., fugacity coefficients, equilibrium constants for homogeneous vapor equilibria, solubility functions for heterogeneous melt-vapor equilibria, saturation conditions, etc.) enable modelling of basaltic through rhyolitic melts, with the hope that new parameterisations will be added as new studies are published. The main calculation types are the pressure of vapor-saturation and range in f_{O2} based on the measured sulfur content from melt inclusion and matrix glass data; as well as open- and closed-system

re- and degassing paths. We applied VolFe calculations to data from the Marianas arc to illustrate the types of results that can be calculated from melt inclusion and submarine pillow glass data.

8 Author contributions

ECH and EMS conceived the project. ECH is the main developer of VolFe with support from PL and PW and input on direction from EMS. ECH wrote the first draft of the manuscript and all authors contributed to subsequent drafts.

9 Acknowledgements

We thank two anonymous reviewers and Meng Tian for their thorough and constructive comments, and Kayla Iacovino for their editorial handling and comments, that greatly improved both the manuscript and Python package. ECH was funded by a Caltech Geology Option Post-Doctoral Fellowship and a Caltech Centre for Comparative Planetary Evolution (^{3}CPE) research grant and is supported by the New Zealand Ministry of Business, Innovation and Employment (MBIE) through the Hazards and Risk Management (Strategic Science Investment Fund, contract C05X1702). PL acknowledges an Embiricos Trust scholarship from Jesus College, University of Cambridge. PW acknowledges funding from a Sloan Research Fellowship.

10 Data availability

VolFe is freely available on github (https://github.com/eryhughes/VolFe), installable using PyPI (the version number should be stated for calculations used), there is documentation on ReadTheDocs (https://volfe.readthedocs.io/en/latest/), and the code is archived in Zenodo (REF).

11 References

Aiuppa, A., Bitetto, M., Calabrese, S., Delle Donne, D., Lages, J., La Monica, F.P., Chiodini, G., Tamburello, G., Cotterill, A., Fulignati, P., Gioncada, A., Liu, E.J., Moretti, R., Pistolesi, M., 2022. Mafic magma feeds degassing unrest at Vulcano Island, Italy. Commun. Earth Environ. 2022 31 3, 1–15. https://doi.org/10.1038/s43247-022-00589-1

Allison, C.M., Roggensack, K., Clarke, A.B., 2022. MafiCH: a general model for H2O–CO2 solubility in mafic magmas. Contrib. to Mineral. Petrol. 177, 1–22. https://doi.org/10.1007/S00410-022-01903-Y/FIGURES/10

Anderson, A.T.J., Newman, S., Williams, S.N., Druitt, T.H., Skirius, C., Stolper, E.M., 1989. H2O, CO2, CI, and gas in Plinian and ash-flow Bishop rhyolite. Geology 17, 221–225. https://doi.org/10.1130/0091-7613(1989)017

Anderson, A.T.J., Wright, T.L., 1972. Phenocrysts and glass inclusions and their bearing on oxidation and mixing of basaltic magmas, kilauea volcano, hawaii. Am. Mineral. 57, 188–216.

Applegarth, L.J., Tuffen, H., James, M.R., Pinkerton, H., 2013. Degassing-driven crystallisation in basalts. Earth-Science Rev. 116, 1–16. https://doi.org/10.1016/J.EARSCIREV.2012.10.007

Ardia, P., Hirschmann, M.M., Withers, A.C., Stanley, B.D., 2013. Solubility of CH4 in a synthetic basaltic melt, with applications to atmosphere–magma ocean–core partitioning of volatiles and to the evolution of the Martian atmosphere. Geochim. Cosmochim. Acta 114, 52–71. https://doi.org/10.1016/J.GCA.2013.03.028

Armstrong, L.S., Hirschmann, M.M., Stanley, B.D., Falksen, E.G., Jacobsen, S.D., 2015. Speciation and solubility of reduced C-O-H-N volatiles in mafic melt: Implications for volcanism, atmospheric evolution, and deep volatile cycles in the terrestrial planets. Geochim. Cosmochim. Acta 171, 283–302. https://doi.org/10.1016/j.gca.2015.07.007

Aubaud, C., Pineau, F., Jambon, A., Javoy, M., 2004. Kinetic disequilibrium of C, He, Ar and carbon isotopes during degassing of mid-ocean ridge basalts. Earth Planet. Sci. Lett. 222, 391–406. https://doi.org/10.1016/j.epsl.2004.03.001

Baker, D.R., Moretti, R., 2011. Modeling the Solubility of Sulfur in Magmas: A 50-Year Old Geochemical Challenge. Rev. Mineral. Geochemistry 73, 167–213. https://doi.org/10.2138/RMG.2011.73.7

Baumgartner, R.J., Baratoux, D., Gaillard, F., Fiorentini, M.L., 2017. Numerical modelling of erosion and assimilation of sulfur-rich substrate by martian lava flows: Implications for the genesis of massive sulfide mineralization on Mars. Icarus 296, 257–274. https://doi.org/10.1016/j.icarus.2017.06.016

Beermann, O., Botcharnikov, R.E., Holtz, F., Diedrich, O., Nowak, M., 2011. Temperature dependence of sulfide and sulfate solubility in olivine-saturated basaltic magmas. Geochim. Cosmochim. Acta 75, 7612–7631. https://doi.org/10.1016/j.gca.2011.09.024

Behrens, H., Ohlhorst, S., Holtz, F., Champenois, M., 2004. CO2 solubility in dacitic melts equilibrated with H2O-CO2 fluids: Implications for modeling the solubility of CO2 in silicic melts. Geochim. Cosmochim. Acta 68, 4687–4703. https://doi.org/10.1016/J.GCA.2004.04.019

Belgrano, T.M., Tollan, P.M., Marxer, F., Diamond, L.W., 2021. Paleobathymetry of Submarine Lavas in the Samail and Troodos Ophiolites: Insights From Volatiles in Glasses and Implications for Hydrothermal Systems. J. Geophys. Res. Solid Earth 126, e2021JB021966. https://doi.org/10.1029/2021JB021966

Belonoshko, A.B., Saxena, S.K., 1992. A unified equation of state for fluids of C-H-O-N-S-Ar composition and their mixtures up to very high temperatures and pressures. Geochim. Cosmochim. Acta 56, 3611–3626. https://doi.org/10.1016/0016-7037(92)90157-E

Black, B.A., Andrews, B.J., 2020. Petrologic imaging of the architecture of magma reservoirs feeding caldera-forming eruptions. Earth Planet. Sci. Lett. 552, 116572.

https://doi.org/10.1016/J.EPSL.2020.116572
Blank, J.G., Brooker, R.A., 1994. Experimental studies of carbon dioxide in silicate melts: Solubility, speciation, and stable carbon isotope behaviour. Rev. Mineral. Geochemistry 30, 157–186.
Blank, J.G., Stolper, E.M., Carroll, M.R., 1993. Solubilities of carbon dioxide and water in rhyolitic melt at 850°C and 750 bars. Earth Planet. Sci. Lett. 119, 27–36. https://doi.org/10.1016/0012-821X(93)90004-S
Blundy, J.D., Cashman, K.V., 2008. Petrologic reconstruction of magmatic system variables and processes. Rev. Mineral. Geochemistry 69, 179–239.
Borisov, A., Behrens, H., Holtz, F., 2018. Ferric/ferrous ratio in silicate melts: a new model for 1 atm data with special emphasis on the effects of melt composition. Contrib. to Mineral. Petrol. 173, 1–15. https://doi.org/10.1007/S00410-018-1524-8/FIGURES/10
Botcharnikov, R.E., Behrens, H., Holtz, F., 2006. Solubility and speciation of C–O–H fluids in andesitic melt at T = 1100–1300 °C and P = 200 and 500 MPa. Chem. Geol. 229, 125–143. https://doi.org/10.1016/J.CHEMGEO.2006.01.016
Boulliung, J., Wood, B.J., 2023a. Sulfur oxidation state and solubility in silicate melts. Contrib. to Mineral. Petrol. 178, 1–15. https://doi.org/10.1007/S00410-023-02033-9/FIGURES/9
Boulliung, J., Wood, B.J., 2023b. Corrigendum to “SO2 solubility and degassing behavior in silicate melts” [Geochim. Cosmochim. Acta 336 (2022) 150–164]. Geochim. Cosmochim. Acta 343, 420. https://doi.org/10.1016/J.GCA.2022.11.025
Boulliung, J., Wood, B.J., 2022. SO2 solubility and degassing behavior in silicate melts. Geochim. Cosmochim. Acta Vol. , 1 Novemb. 2022, Pages 150-164 336, 150–164. https://doi.org/10.1016/j.gca.2022.08.032
Brooker, R.A., Kohn, S.C., Holloway, J.R., McMillan, P.F., Carroll, M.R., 1999. Solubility, speciation and dissolution mechanisms for CO2 in melts on the NaAlO2-SiO2 join. Geochim. Cosmochim. Acta 63, 3549–3565.
Brounce, M.N., Kelley, K.A., Cottrell, E., 2014. Variations in Fe3+/∑Fe of Mariana Arc Basalts and Mantle Wedge fO2. J. Petrol. 55, 2513–2536. https://doi.org/10.1093/PETROLOGY/EGU065
Brounce, M.N., Stolper, E.M., Eiler, J.M., 2017. Redox variations in Mauna Kea lavas, the oxygen fugacity of the Hawaiian plume, and the role of volcanic gases in Earth’s oxygenation. Proc. Natl. Acad. Sci. U. S. A. 114. https://doi.org/10.1073/pnas.1619527114
Burgisser, A., Alletti, M., Scaillet, B., 2015. Simulating the behavior of volatiles belonging to the C–O–H–S system in silicate melts under magmatic conditions with the software D-Compress. Comput. Geosci. 79, 1–14. https://doi.org/10.1016/J.CAGEO.2015.03.002
Burgisser, A., Scaillet, B., 2007. Redox evolution of a degassing magma rising to the surface. Nature 445, 194–197. https://doi.org/10.1038/nature05509
Burnham, C.W., 1979. The importance of volatile constituents, in: Yoder Jr, H.S. (Ed.), The Evolution of the Igneous Rocks: Fiftieth Anniversary Perspectives. University Press, Princeton,

938 Princeton, pp. 439–482.
939 Burnham, C.W., Davis, N.F., 1974. The role of H 2 O in silicate melts; II, Thermodynamic and phase
940 relations in the system NaAlSi 3 O 8 -H 2 O to 10 kilobars, 700 degrees to 1100 degrees C. Am.
941 J. Sci. 274, 902–940. https://doi.org/10.2475/AJS.274.8.902
942 Burton, M., Aiuppa, A., Allard, P., Asensio-Ramos, M., Cofrades, A.P., La Spina, A., Nicholson, E.J.,
943 Zanon, V., Barrancos, J., Bitetto, M., Hartley, M., Romero, J.E., Waters, E., Stewart, A.,
944 Hernández, P.A., Lages, J.P., Padrón, E., Wood, K., Esse, B., Hayer, C., Cyrzan, K., Rose-Koga,
945 E.F., Schiavi, F., D'Auria, L., Pérez, N.M., 2023. Exceptional eruptive CO2 emissions from
946 intra-plate alkaline magmatism in the Canary volcanic archipelago. Commun. Earth Environ.
947 2023 41 4, 1–10. https://doi.org/10.1038/s43247-023-01103-x
948 Camejo-Harry, M., Melekhova, E., Blundy, J., Attridge, W., Robertson, R., Christopher, T., 2018.
949 Magma evolution beneath Bequia, Lesser Antilles, deduced from petrology of lavas and plutonic
950 xenoliths. Contrib. to Mineral. Petrol. 173, 1–26. https://doi.org/10.1007/S00410-018-1504-
951 Z/FIGURES/14
952 Camejo-Harry, M., Melekhova, E., Blundy, J., Robertson, R., 2019. Evolution in magma storage
953 conditions beneath Kick-'em-Jenny and Kick-'em-Jack submarine volcanoes, Lesser Antilles
954 arc. J. Volcanol. Geotherm. Res. 373, 1–22.
955 https://doi.org/10.1016/J.JVOLGEORES.2019.01.023
956 Candela, P.A., 1986. The evolution of aqueous vapor from silicate melts: Effect on oxygen fugacity.
957 Geochim. Cosmochim. Acta 50, 1205–1211. https://doi.org/10.1016/0016-7037(86)90403-5
958 Carey, R.J., Manga, M., Degruyter, W., Gonnermann, H., Swanson, D., Houghton, B., Orr, T.,
959 Patrick, M., 2013. Convection in a volcanic conduit recorded by bubbles. Geology 41, 395–398.
960 https://doi.org/10.1130/G33685.1
961 Carmichael, I.S.E., Ghiorso, M.S., 1990. The effect of oxygen fugacity on the redox state of natural
962 liquids and their crystallizing phases. Rev. Mineral. Geochemistry 24, 191–212.
963 Carmichael, I.S.E., Ghiorso, M.S., 1986. Oxidation-reduction relations in basic magma: a case for
964 homogeneous equilibria. Earth Planet. Sci. Lett. 78, 200–210. https://doi.org/10.1016/0012-
965 821X(86)90061-0
966 Chowdhury, P., Dasgupta, R., 2019. Effect of sulfate on the basaltic liquidus and Sulfur Concentration
967 at Anhydrite Saturation (SCAS) of hydrous basalts – Implications for sulfur cycle in subduction
968 zones. Chem. Geol. 522, 162–174. https://doi.org/10.1016/J.CHEMGEO.2019.05.020
969 Clemente, B., SCAILLET, B., PICHAVANT, M., 2004. The Solubility of Sulphur in Hydrous
970 Rhyolitic Melts. J. Petrol. 45, 2171–2196. https://doi.org/10.1093/petrology/egh052
971 Colman, A., Sinton, J.M., Wanless, V.D., 2015. Constraints from melt inclusions on depths of magma
972 residence at intermediate magma supply along the Galápagos Spreading Center. Earth Planet.
973 Sci. Lett. 412, 122–131. https://doi.org/10.1016/J.EPSL.2014.12.007
974 Coombs, M.L., Sisson, T.W., Lipman, P.W., 2006. Growth history of Kilauea inferred from volatile

concentrations in submarine-collected basalts. J. Volcanol. Geotherm. Res. 151, 19–49. https://doi.org/10.1016/J.JVOLGEORES.2005.07.037

Cottrell, E., Birner, S.K., Brounce, M., Davis, F.A., Waters, L.E. and Kelley, K.A., 2021. Oxygen fugacity across tectonic settings. *Magma redox geochemistry*, pp.33-61. https://doi.org/10.1002/9781119473206.ch3

Denbigh, K., 1971, The Principles of Chemical Equilibrium (Third Edition), Cambridge University Press, 494 pp.

Ding, S., Plank, T., Wallace, P.J., Rasmussen, D.J., 2023. Sulfur_X: A Model of Sulfur Degassing During Magma Ascent. Geochemistry, Geophys. Geosystems 24, e2022GC010552. https://doi.org/10.1029/2022GC010552

Dingwell, D.B., Romano, C., Hess, K.U., 1996. The effect of water on the viscosity of a haplogranitic melt under P-T-X conditions relevant to silicic volcanism. Contrib. to Mineral. Petrol. 124, 19–28. https://doi.org/10.1007/S004100050170/METRICS

Dixon, J.E., 1997. Degassing of alkalic basalts. Am. Mineral. 82, 368–378. https://doi.org/10.2138/AM-1997-3-415/MACHINEREADABLECITATION/RIS

Dixon, J.E., Stolper, E.M., 1995. An experimental study water and carbon dioxide solubilities in mid-ocean ridge basaltic liquids. Part II: Application to degassing. J. Petrol. 36, 1633–1646.

Dixon, J.E., Stolper, E.M., Holloway, J.R., 1995. An experimental study of water and carbon dioxide solubilities in mid-ocean ridge basaltic liquids. Part I: Calibration and solubility models. J. Petrol. 36, 1607–1631. https://doi.org/10.1093/oxfordjournals.petrology.a037267

Duan, Z., Zhang, Z., 2006. Equation of state of the H2O, CO2, and H2O–CO2 systems up to 10 GPa and 2573.15 K: Molecular dynamics simulations with ab initio potential surface. Geochim. Cosmochim. Acta 70, 2311–2324. https://doi.org/10.1016/J.GCA.2006.02.009

Fincham, C.J.B., Richardson, F.D., 1954. The behaviour of sulphur in silicate and aluminate melts. Proc. R. Soc. London. Ser. A. Math. Phys. Sci. 223, 40–62. https://doi.org/10.1098/rspa.1954.0099

Fine, G., Stolper, E., 1986. Dissolved carbon dioxide in basaltic glasses: concentrations and speciation. Earth Planet. Sci. Lett. 76, 263–278. https://doi.org/10.1016/0012-821X(86)90078-6

Fine, G., Stolper, E., 1985. The speciation of carbon dioxide in sodium aluminosilicate glasses. Contrib. to Mineral. Petrol. 91, 105–121. https://doi.org/10.1007/BF00377759/METRICS

Flowers, G.C., 1979. Correction of Holloway's (1977) adaptation of the modified Redlich-Kwong equation of state for calculation of the fugacities of molecular species in supercritical fluids of geologic interest. *Contributions to Mineralogy and Petrology*, *69*(3), pp.315-318.

Fortin, M.A., Riddle, J., Desjardins-Langlais, Y., Baker, D.R., 2015. The effect of water on the sulfur concentration at sulfide saturation (SCSS) in natural melts. Geochim. Cosmochim. Acta 160, 100–116. https://doi.org/10.1016/J.GCA.2015.03.022

Frost, B.R., 1991. Introduction to oxygen fugacity and its petrologic importance. Rev. Mineral.

Geochemistry 25, 1–9.
Gaillard, F., Michalski, J., Berger, G., McLennan, S.M., Scaillet, B., 2013. Geochemical reservoirs and timing of sulfur cycling on Mars. Space Sci. Rev. https://doi.org/10.1007/s11214-012-9947-4
Gaillard, F., Scaillet, B., 2014. A theoretical framework for volcanic degassing chemistry in a comparative planetology perspective and implications for planetary atmospheres. Earth Planet. Sci. Lett. 403, 307–316. https://doi.org/10.1016/j.epsl.2014.07.009
Gaillard, F., Scaillet, B., 2009. The sulfur content of volcanic gases on Mars. Earth Planet. Sci. Lett. 279, 34–43. https://doi.org/10.1016/J.EPSL.2008.12.028
Gaillard, F., Scaillet, B., Arndt, N.T., 2011. Atmospheric oxygenation caused by a change in volcanic degassing pressure. Nature 478, 229–232. https://doi.org/10.1038/nature10460
Gaillard, F., Scaillet, B., Pichavant, M., Iacono-Marziano, G., 2015. The redox geodynamics linking basalts and their mantle sources through space and time. Chem. Geol. 418, 217–233. https://doi.org/10.1016/j.chemgeo.2015.07.030
Gaillard, F., Schmidt, B., Mackwell, S., McCammon, C., 2003. Rate of hydrogen–iron redox exchange in silicate melts and glasses. Geochim. Cosmochim. Acta 67, 2427–2441. https://doi.org/10.1016/s0016-7037(02)01407-2
Ghiorso, M.S., Gualda, G.A.R., 2015. An H2O–CO2 mixed fluid saturation model compatible with rhyolite-MELTS. Contrib. to Mineral. Petrol. 169, 53. https://doi.org/10.1007/s00410-015-1141-8
Ghiorso, M.S., Matthews, S., Sverjensky, D.A., 2023. MELTS+DEW: Modeling major element+Cl+F+S phase equilibria, redox reactions and elemental partitioning in magmatic-hydrothermal systems, in: Goldschmidt.
Gibbs, J.W., 1978. On the Equilibrium of Heterogeneous Substances. Trans. Connect. Acad. Arts Sci. 3, 343–524.
Gibbs, J.W., 1976. On the Equilibrium of Heterogeneous Substances. Trans. Connect. Acad. Arts Sci. 3, 108–248.
Gualda, G.A.R., Ghiorso, M.S., Lemons, R. V., Carley, T.L., 2012. Rhyolite-MELTS: a Modified Calibration of MELTS Optimized for Silica-rich, Fluid-bearing Magmatic Systems. J. Petrol. 53, 875–890. https://doi.org/10.1093/PETROLOGY/EGR080
Hartley, M.E., Maclennan, J., Edmonds, M. and Thordarson, T., 2014. Reconstructing the deep CO2 degassing behaviour of large basaltic fissure eruptions. *Earth and Planetary Science Letters*, *393*, pp.120-131. https://doi.org/10.1016/j.epsl.2014.02.031
Hirschmann, M.M., Withers, A.C., Ardia, P., Foley, N.T., 2012. Solubility of molecular hydrogen in silicate melts and consequences for volatile evolution of terrestrial planets. Earth Planet. Sci. Lett. 345–348, 38–48. https://doi.org/10.1016/J.EPSL.2012.06.031
Holland, T., Powell, R., 1991. A Compensated-Redlich-Kwong (CORK) equation for volumes and

fugacities of CO2 and H2O in the range 1 bar to 50 kbar and 100–1600°C. Contrib. to Mineral. Petrol. 1991 1092 109, 265–273. https://doi.org/10.1007/BF00306484

Holloway, J.R., 1977. Fugacity and Activity of Molecular Species in Supercritical Fluids, in: Thermodynamics in Geology. Springer Netherlands, Dordrecht, pp. 161–181. https://doi.org/10.1007/978-94-010-1252-2_9

Holloway, J.R., Blank, J.G., 1994. Application of experimental results to C-O-H species in natural melts. Rev. Mineral. Geochemistry1 30, 187–230.

Holloway, J.R., Pan, V., Gudmundsson, G.B., 1992. High-pressure fluid-absent melting experiments in the presence of graphite: oxygen fugacity, ferric/ferrous ratio and dissolved CO2. Eur. J. Mineral. 4, 105–114.

Hughes, E.C., Ding, S., Iacovino, K., Wieser, P.E., Kilgour, G., 2023. Workshop report: Modelling volatile behaviour in magmas. Earth ArXiv. https://doi.org/10.31223/X5FD3Q

Hughes, E.C., Liggins, P., Saper, L., Stolper, E.M., 2024. The effects of oxygen fugacity and sulfur on the pressure of vapor-saturation of magma. Am. Mineral. 109, 422–438.

Hughes, E.C., Saper, L.M., Liggins, P., O'Neill, H.S.C., Stolper, E.M., 2022. The sulfur solubility minimum and maximum in silicate melt. J. Geol. Soc. London. 180, jgs2021-125. https://doi.org/https://doi.org/10.1144/jgs2021-125

Iacono-Marziano, G., Morizet, Y., Le Trong, E., Gaillard, F., 2012a. New experimental data and semi-empirical parameterization of H2O–CO2 solubility in mafic melts. Geochim. Cosmochim. Acta 97, 1–23. https://doi.org/10.1016/J.GCA.2012.08.035

Iacono-Marziano, G., Morizet, Y., Le Trong, E., Gaillard, F., 2012b. New experimental data and semi-empirical parameterization of H2O–CO2 solubility in mafic melts. Geochim. Cosmochim. Acta 97, 1–23. https://doi.org/10.1016/J.GCA.2012.08.035

Iacono-Marziano, G., Paonita, A., Rizzo, A., Scaillet, B., Gaillard, F., 2010. Noble gas solubilities in silicate melts: New experimental results and a comprehensive model of the effects of liquid composition, temperature and pressure. Chem. Geol. 279, 145–157. https://doi.org/10.1016/J.CHEMGEO.2010.10.017

Iacovino, K., 2015. Linking subsurface to surface degassing at active volcanoes: a thermodynamic model with applications to Erebus volcano. *Earth and Planetary Science Letters*, *431*, pp.59-74. https://doi.org/10.1016/j.epsl.2015.09.016

Iacovino, K., Matthews, S., Wieser, P.E., Moore, G.M., Bégué, F., 2021. VESIcal Part I: An open-source thermodynamic model engine for mixed volatile (O-) solubility in silicate melts. Earth Sp. Sci. e2020EA001584. https://doi.org/10.1029/2020EA001584

Iacovino, K., Till, C., 2018. DensityX: A program for calculating the densities of hydrous magmatic liquids from 427-1,627 °C and up to 30 kbar. Volcanica 2, 1–10. https://doi.org/10.30909/vol.02.01.0110

Jugo, P.J., Wilke, M., Botcharnikov, R.E., 2010. Sulfur K-edge XANES analysis of natural and

synthetic basaltic glasses: Implications for S speciation and S content as function of oxygen fugacity. Geochim. Cosmochim. Acta 74, 5926–5938. https://doi.org/10.1016/J.GCA.2010.07.022

Kadik, A.A., Lukanin, O.A., Lebedev, Y.B., Korovushkina, E.Y., 1972. Solubility of H2O and CO2 in granite and basalt melts at high pressures. Geochem. Int. 9, 1041–1050.

Kadik, A.A., Pineau, F., Litvin, Y., Jendrzejewski, N., Martinez, I., Javoy, M., 2004. Formation of Carbon and Hydrogen Species in Magmas at Low Oxygen Fugacity. J. Petrol. 45, 1297–1310. https://doi.org/10.1093/PETROLOGY/EGH007

Kelley, K.A., Cottrell, E., 2012. The influence of magmatic differentiation on the oxidation state of Fe in a basaltic arc magma. Earth Planet. Sci. Lett. 329–330, 109–121. https://doi.org/10.1016/j.epsl.2012.02.010

Kern, C., Aiuppa, A., de Moor, J.M., 2022. A golden era for volcanic gas geochemistry? Bull. Volcanol. 2022 845 84, 1–11. https://doi.org/10.1007/S00445-022-01556-6

King, P.L., Holloway, J.R., 2002. CO2 solubility and speciation in intermediate (andesitic) melts: the role of H2O and composition. Geochim. Cosmochim. Acta 66, 1627–1640. https://doi.org/10.1016/S0016-7037(01)00872-9

Klimm, K., Kohn, S.C., Botcharnikov, R.E., 2012a. The dissolution mechanism of sulphur in hydrous silicate melts. II: Solubility and speciation of sulphur in hydrous silicate melts as a function of fO2. Chem. Geol. 322–323, 250–267. https://doi.org/10.1016/J.CHEMGEO.2012.04.028

Klimm, K., Kohn, S.C., O'Dell, L.A., Botcharnikov, R.E., Smith, M.E., 2012b. The dissolution mechanism of sulphur in hydrous silicate melts. I: Assessment of analytical techniques in determining the sulphur speciation in iron-free to iron-poor glasses. Chem. Geol. 322–323, 237–249. https://doi.org/10.1016/J.CHEMGEO.2012.04.027

Kolzenburg, S., Di Genova, D., Giordano, D., Hess, K.U., Dingwell, D.B., 2018. The effect of oxygen fugacity on the rheological evolution of crystallizing basaltic melts. Earth Planet. Sci. Lett. 487, 21–32. https://doi.org/10.1016/J.EPSL.2018.01.023

Kress, V.C., Carmichael, I.S.E., 1991. The compressibility of silicate liquids containing Fe2O3 and the effect of composition, temperature, oxygen fugacity and pressure on their redox states. Contrib. to Mineral. Petrol. 108, 82–92. https://doi.org/10.1007/BF00307328

Lesne, P., Scaillet, B., Pichavant, M., 2015. The solubility of sulfur in hydrous basaltic melts. Chem. Geol. 418, 104–116. https://doi.org/10.1016/J.CHEMGEO.2015.03.025

Lesne, P., Scaillet, B., Pichavant, M., Brey, G.P., 2011a. The carbon dioxide solubility in alkali basalts: an experimental study. Contrib. to Mineral. Petrol. 162, 153–168. https://doi.org/10.1007/s00410-010-0585-0

Lesne, P., Scaillet, B., Pichavant, M., Iacono-Marziano, G., Beny, J.M., 2011b. The H2O solubility of alkali basaltic melts: An experimental study. Contrib. to Mineral. Petrol. 162, 133–151. https://doi.org/10.1007/S00410-010-0588-X/FIGURES/12

Liggins, P., Jordan, S., Rimmer, P.B., Shorttle, O., 2022. Growth and Evolution of Secondary Volcanic Atmospheres: I. Identifying the Geological Character of Hot Rocky Planets. J. Geophys. Res. Planets 127, e2021JE007123. https://doi.org/10.1029/2021JE007123

Liggins, P., Shorttle, O., Rimmer, P.B., 2020. Can volcanism build hydrogen-rich early atmospheres? Earth Planet. Sci. Lett. 550, 116546. https://doi.org/10.1016/J.EPSL.2020.116546

Liu, K., Zhang, L., Guo, X., Ni, H., 2021. Effects of sulfide composition and melt H2O on sulfur content at sulfide saturation in basaltic melts. Chem. Geol. 559, 119913. https://doi.org/10.1016/j.chemgeo.2020.119913

Liu, Y., Samaha, N.T., Baker, D.R., 2007. Sulfur concentration at sulfide saturation (SCSS) in magmatic silicate melts. Geochim. Cosmochim. Acta 71, 1783–1799. https://doi.org/10.1016/J.GCA.2007.01.004

Lund, D.C., Seeley, E.I., Asimow, P.D., Lewis, M.J., McCart, S.E., Mudahy, A.A., 2018. Anomalous Pacific-Antarctic Ridge Volcanism Precedes Glacial Termination 2. Geochemistry, Geophys. Geosystems 19, 2478–2491. https://doi.org/10.1029/2017GC007341

Lux, G., 1987. The behavior of noble gases in silicate liquids: Solution, diffusion, bubbles and surface effects, with applications to natural samples. Geochim. Cosmochim. Acta 51, 1549–1560. https://doi.org/10.1016/0016-7037(87)90336-X

Macpherson, C.G., Mattey, D.P., 1994. Carbon isotope variations of CO2 in Central Lau Basin basalts and ferrobasalts. Earth Planet. Sci. Lett. 121, 263–276. https://doi.org/10.1016/0012-821X(94)90072-8

Marshall, L.R., Maters, E.C., Schmidt, A., Timmreck, C., Robock, A., Toohey, M., 2022. Volcanic effects on climate: recent advances and future avenues. Bull. Volcanol. 2022 845 84, 1–14. https://doi.org/10.1007/S00445-022-01559-3

Matthews, S.J., Moncrieff, D.H.S., Carroll, M.R., 1999. Empirical Calibration of the Sulphur Valence Oxygen Barometer from Natural and Experimental Glasses: Method and Applications. Mineral. Mag. 63, 421–431. https://doi.org/10.1180/002646199548510

Métrich, N., Berry, A.J., O'Neill, H.S.C., Susini, J., 2009. The oxidation state of sulfur in synthetic and natural glasses determined by X-ray absorption spectroscopy. Geochim. Cosmochim. Acta 73, 2382–2399. https://doi.org/10.1016/J.GCA.2009.01.025

Meurer, A., Smith, C., Paprocki, M., Čertík, O., Kirpichev, S., Rocklin, M., Kumar, A., Ivanov, S., Moore, J., Singh, S., Rathnayake, T., Vig, S., Granger, B., Muller, R., Bonazzi, F., Gupta, H., Vats, S., Johansson, F., Pedregosa, F., Curry, M., Terrel, A., Roučka, Š., Saboo, A., Fernando, I., Kulal, S., Cimrman, R., A, S., 2017. SymPy: symbolic computing in Python. PeerJ Comput. Sci. 3, e103.

Moore, G., Vennemann, T., Carmichael, I.S.E., 1998. An empirical model for the solubility of H 2 O in magmas to 3 kilobars. Am. Mineral. 83, 36–42. https://doi.org/10.2138/AM-1998-1-203

Moore, J.G., Fornari, D.J., Clague, D.A., 1985. Basalts from the 1877 submarine eruption of Mauna

Loa, Hawaii; new data on the variation of palagonitization rate with temperature, Bulletin. https://doi.org/10.3133/b1663

Moore, L.R., Bodnar, R.J., 2019. A pedagogical approach to estimating the co2 budget of magmas. J. Geol. Soc. London. 176, 398–407. https://doi.org/10.1144/JGS2018-094/ASSET/FC74300B-06F9-4FA7-85E5-C05E16121F7D/ASSETS/IMAGES/LARGE/JGS2018-094.05.JPG

Moore, L.R., Gazel, E., Tuohy, R., Lloyd, A.S., Esposito, R., Steele-MacInnis, M., Hauri, E.H., Wallace, P.J., Plank, T. and Bodnar, R.J., 2015. Bubbles matter: An assessment of the contribution of vapor bubbles to melt inclusion volatile budgets. *American Mineralogist*, *100*(4), pp.806-823. https://doi.org/10.2138/am-2015-5036

Moretti, R., 2021. Ionic Syntax and Equilibrium Approach to Redox Exchanges in Melts: Basic Concepts and the Case of Iron and Sulfur in Degassing Magmas, in: Moretti, R., Neuville, D.R. (Eds.), Magma Redox Geochemistry, Geophysical Monograph Series. American Geophysical Union (AGU), pp. 115–138. https://doi.org/10.1002/9781119473206.CH6

Moretti, R., Ottonello, G., 2005. Solubility and speciation of sulfur in silicate melts: The Conjugated Toop-Samis-Flood-Grjotheim (CTSFG) model. Geochim. Cosmochim. Acta 69, 801–823. https://doi.org/10.1016/J.GCA.2004.09.006

Moretti, R., Ottonello, G., 2003. Polymerization and disproportionation of iron and sulfur in silicate melts: Insights from an optical basicity-based approach, in: Journal of Non-Crystalline Solids. North-Holland, pp. 111–119. https://doi.org/10.1016/S0022-3093(03)00297-7

Moretti, R., Papale, P., 2004. On the oxidation state and volatile behavior in multicomponent gas-melt equilibria. Chem. Geol. 213, 265–280. https://doi.org/10.1016/j.chemgeo.2004.08.048

Moretti, R., Papale, P., Ottonello, G., 2003. A model for the saturation of C-O-H-S fluids in silicate melts. Geol. Soc. London, Spec. Publ. 213, 81–101. https://doi.org/10.1144/GSL.SP.2003.213.01.06

Moune, S., Holtz, F., Botcharnikov, R.E., 2009. Sulphur solubility in andesitic to basaltic melts: implications for Hekla volcano. Contrib. to Mineral. Petrol. 157, 691–707. https://doi.org/10.1007/s00410-008-0359-0

Moussallam, Y., Edmonds, M., Scaillet, B., Peters, N., Gennaro, M.E., Sides, I., Oppenheimer, C., 2016. The impact of degassing on the oxidation state of basaltic magmas: A case study of Kīlauea volcano. Earth Planet. Sci. Lett. 450, 317–325. https://doi.org/10.1016/j.epsl.2016.06.031

Moussallam, Y., Oppenheimer, C., Scaillet, B., 2022. A novel approach to volcano surveillance using gas geochemistry. Comptes Rendus - Geosci. 355, 1–14. https://doi.org/10.5802/CRGEOS.158/FILE/ATTACH/CRGEOS-158-SUPPL.PDF

Moussallam, Y., Oppenheimer, C., Scaillet, B., 2019. On the relationship between oxidation state and temperature of volcanic gas emissions. Earth Planet. Sci. Lett. 520, 260–267. https://doi.org/10.1016/J.EPSL.2019.05.036

Moussallam, Y., Oppenheimer, C., Scaillet, B., Gaillard, F., Kyle, P., Peters, N., Hartley, M.E., Berlo, K., Donovan, A., 2014. Tracking the changing oxidation state of Erebus magmas, from mantle to surface, driven by magma ascent and degassing. Earth Planet. Sci. Lett. 393, 200–209. https://doi.org/10.1016/j.epsl.2014.02.055

Muth, M.J., Wallace, P.J., 2022. Sulfur recycling in subduction zones and the oxygen fugacity of mafic arc magmas. Earth Planet. Sci. Lett. 599, 117836. https://doi.org/10.1016/J.EPSL.2022.117836

Mysen, B., 2013. Structure–property relationships of COHN-saturated silicate melt coexisting with COHN fluid: A review of in-situ, high-temperature, high-pressure experiments. Chem. Geol. 346, 113–124. https://doi.org/10.1016/J.CHEMGEO.2012.10.006

Mysen, B.O., Kumamoto, K., Cody, G.D., Fogel, M.L., 2011. Solubility and solution mechanisms of C–O–H volatiles in silicate melt with variable redox conditions and melt composition at upper mantle temperatures and pressures. Geochim. Cosmochim. Acta 75, 6183–6199. https://doi.org/10.1016/J.GCA.2011.07.035

Mysen, B.O., Virgo, D., Harrison, W.J., Scarfe, C.M., 1980. Solubility mechanisms of H2O in silicate melts at high pressures and temperatures: a Raman spectroscopic study | American Mineralogist | GeoScienceWorld. Am. Mineral. 65, 900–914.

Newman, S., Epstein, S., Stolper, E.M., 1988. Water, carbon dioxide, and hydrogen isotopes in glasses from the ca. 1340 A.D. eruption of the Mono Craters, California: Constraints on degassing phenomena and initial volatile content. J. Volcanol. Geotherm. Res. 35, 75–96. https://doi.org/10.1016/0377-0273(88)90007-8

Newman, S., Lowenstern, J.B., 2002. VolatileCalc: a silicate melt–H2O–CO2 solution model written in Visual Basic for excel. Comput. Geosci. 28, 597–604. https://doi.org/10.1016/S0098-3004(01)00081-4

O'Neill, H.S.C., 2021. The thermodynamic controls on sulfide saturation in silicate melts with application to Ocean Floor Basalts., in: Moretti, R., Neuville, D.R. (Eds.), Magma Redox Geochemistry, Geophysical Monograph Series. John Wiley & Sons, Inc., pp. 177–213. https://doi.org/10.1002/9781119473206.ch10

O'Neill, H.S.C., 1987. Quartz-fayalite-iron and quartz-fayalite-magnetite equilibria and the free energy of formation of fayalite (Fe2SiO4) and magnetite (Fe3O4). Am. Mineral. 72, 67–75.

O'Neill, H.S.C., Berry, A.J., Mallmann, G., 2018. The oxidation state of iron in Mid-Ocean Ridge Basaltic (MORB) glasses: Implications for their petrogenesis and oxygen fugacities. Earth Planet. Sci. Lett. 504, 152–162. https://doi.org/10.1016/J.EPSL.2018.10.002

O'Neill, H.S.C., Mavrogenes, J.A., 2022. The sulfate capacities of silicate melts. Geochim. Cosmochim. Acta. https://doi.org/10.1016/J.GCA.2022.06.020

O'Neill, H.S.C., Mavrogenes, J.A., 2002. The sulfide capacity and the sulfur content at sulfide saturation of silicate melts at 1400°C and 1 bar. J. Petrol. 43, 1049–1087.

https://doi.org/10.1093/petrology/43.6.1049
Ohmoto, H., Kerrick, D.M., 1977. Devolatilization equilibria in graphitic systems. Am. J. Sci. 277, 1013–1044. https://doi.org/10.2475/AJS.277.8.1013
Papale, P., Moretti, R., Barbato, D., 2006. The compositional dependence of the saturation surface of H2O+CO2 fluids in silicate melts. Chem. Geol. 229, 78–95. https://doi.org/10.1016/j.chemgeo.2006.01.013
Papale, P., Moretti, R., Paonita, A., 2022. Thermodynamics of Multi-component Gas–Melt Equilibrium in Magmas: Theory, Models, and Applications. Rev. Mineral. Geochemistry 87, 431–556. https://doi.org/10.2138/RMG.2022.87.10
Paris, E., Giuli, G., Carroll, M.R., Davoli, I., 2001. The valence and speciation of sulfur in glasses by X-ray absorption spectroscopy. Can. Mineral. 39, 331–339. https://doi.org/10.2113/gscanmin.39.2.331
Powell, R., Holland, T.J.B.H. and Worley, B., 1998. Calculating phase diagrams involving solid solutions via non-linear equations, with examples using THERMOCALC. *Journal of metamorphic Geology*, *16*(4), pp.577-588. https://doi.org/10.1111/j.1525-1314.1998.00157.x
Prigogine, I., Defay, R., 1954. Treatise on Thermodynamics Based on the Methods of Gibbs and De Donder. Longmans, Green, London.
Putirka, K.D., 2008. Thermometers and Barometers for Volcanic Systems. Rev. Mineral. Geochemistry 69, 61–120. https://doi.org/10.2138/rmg.2008.69.3
Ranta, E., Halldórsson, S.A., Óladóttir, B.A., Pfeffer, M.A., Caracciolo, A., Bali, E., Guðfinnsson, G.H., Kahl, M., Barsotti, S., 2024. Magmatic Controls on Volcanic Sulfur Emissions at the Iceland Hotspot. Geochemistry, Geophys. Geosystems 25, e2024GC011443. https://doi.org/10.1029/2024GC011443
Rasmussen, D.J., Plank, T.A., Wallace, P.J., Newcombe, M.E., Lowenstern, J.B., 2020. Vapor-bubble growth in olivine-hosted melt inclusions. Am. Mineral. 105, 1898–1919. https://doi.org/10.2138/AM-2020-7377
Rose-Koga, E.F., Bouvier, A.S., Gaetani, G.A., Wallace, P.J., Allison, C.M., Andrys, J.A., Angeles de la Torre, C.A., Barth, A., Bodnar, R.J., Bracco Gartner, A.J.J., Butters, D., Castillejo, A., Chilson-Parks, B., Choudhary, B.R., Cluzel, N., Cole, M., Cottrell, E., Daly, A., Danyushevsky, L. V., DeVitre, C.L., Drignon, M.J., France, L., Gaborieau, M., Garcia, M.O., Gatti, E., Genske, F.S., Hartley, M.E., Hughes, E.C., Iveson, A.A., Johnson, E.R., Jones, M., Kagoshima, T., Katzir, Y., Kawaguchi, M., Kawamoto, T., Kelley, K.A., Koornneef, J.M., Kurz, M.D., Laubier, M., Layne, G.D., Lerner, A.H., Lin, K.Y., Liu, P.P., Lorenzo-Merino, A., Luciani, N., Magalhães, N., Marschall, H.R., Michael, P.J., Monteleone, B.D., Moore, L.R., Moussallam, Y., Muth, M., Myers, M.L., Narváez, D.F., Navon, O., Newcombe, M.E., Nichols, A.R.L., Nielsen, R.L., Pamukcu, A., Plank, T., Rasmussen, D.J., Roberge, J., Schiavi, F., Schwartz, D., Shimizu, K., Shimizu, N., Thomas, J.B., Thompson, G.T., Tucker, J.M., Ustunisik, G., Waelkens, C.,

Zhang, Y., Zhou, T., 2021. Silicate melt inclusions in the new millennium: A review of recommended practices for preparation, analysis, and data presentation. Chem. Geol. 570, 120145. https://doi.org/10.1016/j.chemgeo.2021.120145

Sack, R.O., Carmichael, I.S.E., Rivers, M., Ghiorso, M.S., 1981. Ferric-ferrous equilibria in natural silicate liquids at 1 bar. Contrib. to Mineral. Petrol. 75, 369–376. https://doi.org/10.1007/BF00374720/METRICS

Seaman, C., Sherman, S.B., Garcia, M.O., Baker, M.B., Balta, B., Stolper, E.M., 2004. Volatiles in glasses from the HSDP2 drill core. Geochemistry, Geophys. Geosystems 5. https://doi.org/10.1029/2003GC000596

Shaw, H.R., Wones, D.R., 1964. Fugacity coefficients for hydrogen gas between 0 degrees and 1000 degrees C, for pressures to 3000 atm. Am. J. Sci. 262, 918–929. https://doi.org/10.2475/AJS.262.7.918

Shi, P., Saxena, S.K., 1992. Thermodynamic modeing of the C-H-O-S fluid system. Am. Mineral. 77, 1038–1049.

Shishkina, T.A., Botcharnikov, R.E., Holtz, F., Almeev, R.R., Jazwa, A.M., Jakubiak, A.A., 2014. Compositional and pressure effects on the solubility of H2O and CO2 in mafic melts. Chem. Geol. 388, 112–129. https://doi.org/10.1016/J.CHEMGEO.2014.09.001

Silver, L.A., Ihinger, P.D., Stolper, E.M., 1990. The influence of bulk composition on the speciation of water in silicate glasses. Contrib. to Mineral. Petrol. 104, 142–162. https://doi.org/10.1007/BF00306439

Silver, L.A., Stolper, E.M., 1989. Water in albitic glasses. J. Petrol. 30, 667–709. https://doi.org/10.1093/petrology/30.3.667

Simon, A.C., Ripley, E.M., 2011. The Role of Magmatic Sulfur in the Formation of Ore Deposits. Rev. Mineral. Geochemistry 73, 513–578. https://doi.org/10.2138/RMG.2011.73.16

Smythe, D.J., Wood, B.J., Kiseeva, E.S., 2017. The S content of silicate melts at sulfide saturation: New experiments and a model incorporating the effects of sulfide composition. Am. Mineral. 102, 795–803. https://doi.org/10.2138/AM-2017-5800CCBY

Soule, S.A., Nakata, D.S., Fornari, D.J., Fundis, A.T., Perfit, M.R., Kurz, M.D., 2012. CO2 variability in mid-ocean ridge basalts from syn-emplacement degassing: Constraints on eruption dynamics. Earth Planet. Sci. Lett. 327–328, 39–49. https://doi.org/10.1016/J.EPSL.2012.01.034

Spera, F.J., Bergman, S.C., 1980. Carbon Dioxide in igneous petrogenesis: I. Contrib. to Mineral. Petrol. 74, 55–66. https://doi.org/10.1007/BF00375489

Stanley, B.D., Hirschmann, M.M., Withers, A.C., 2014. Solubility of COH volatiles in graphite-saturated martian basalts. Geochim. Cosmochim. Acta 129, 54–76. https://doi.org/10.1016/j.gca.2013.12.013

Stewart, C., Damby, D.E., Horwell, C.J., Elias, T., Ilyinskaya, E., Tomašek, I., Longo, B.M., Schmidt, A., Carlsen, H.K., Mason, E., Baxter, P.J., Cronin, S., Witham, C., 2021. Volcanic air pollution

and human health: recent advances and future directions. Bull. Volcanol. 2021 841 84, 1–25. https://doi.org/10.1007/S00445-021-01513-9

Stolper, E.M., 1982a. Water in silicate glasses: An infrared spectroscopic study. Contrib. to Mineral. Petrol. 81, 1–17. https://doi.org/10.1007/BF00371154

Stolper, E.M., 1982b. The speciation of water in silicate melts. Geochim. Cosmochim. Acta 46, 2609–2620.

Stolper, E.M., Fine, G., Johnson, T., Newman, S., 1987. Solubility of carbon dioxide in albitic melt. Am. Mineral. 72, 1071–1085.

Stolper, E.M., Holloway, J.R., 1988a. Experimental determination of the solubility of carbon dioxide in molten basalt at low pressure. Earth Planet. Sci. Lett. 87.

Stolper, E.M., Holloway, J.R., 1988b. Experimental determination of the solubility of carbon dioxide in molten basalt at low pressure. Earth Planet. Sci. Lett. 87, 397–408. https://doi.org/10.1016/0012-821X(88)90004-0

Sun, C., Lee, C.-T.A., 2022. Redox evolution of crystallizing magmas with C-H-O-S volatiles and its implications for atmospheric oxygenation. Geochim. Cosmochim. Acta 338, 302–321.

Sun, C., Yao, L., 2024. Redox equilibria of iron in low- to high-silica melts: A simple model and its applications to C-H-O-S degassing. Earth Planet. Sci. Lett. 638, 118742. https://doi.org/10.1016/J.EPSL.2024.118742

Taracsák, Z., Mather, T.A., Ding, S., Plank, T., Brounce, M., Pyle, D.M., Aiuppa, A., EIMF, 2023. Sulfur from the subducted slab dominates the sulfur budget of the mantle wedge under volcanic arcs. Earth Planet. Sci. Lett. 602, 117948. https://doi.org/10.1016/J.EPSL.2022.117948

Thibault, Y., Holloway, J.R., 1994. Solubility of CO2 in a Ca-rich leucitite: effects of pressure, temperature, and oxygen fugacity. Contrib. to Mineral. Petrol. 116, 216–224. https://doi.org/10.1007/BF00310701/METRICS

Thomas, R.W., Wood, B.J., 2022. The effect of composition on chlorine solubility and behaviour in silicate melts. Am. Mineral.

Wallace, P.J., Carmichael, I.S.E., 1994. S speciation in submarine basaltic glasses as determined by measurements of SKa X-ray wavelength shifts. Am. Mineral. 79, 161–167.

Wallace, P.J., Kamenetsky, V.S. and Cervantes, P., 2015. Melt inclusion CO2 contents, pressures of olivine crystallization, and the problem of shrinkage bubbles. *American Mineralogist*, *100*(4), pp.787-794. https://doi.org/10.2138/am-2015-5029

Walter, S.C., Castro, J.M., 2020. VolcDeGas: A program for modelling hydrogen isotope fractionation during degassing of rhyolitic melts. Volcanica 3, 155–168. https://doi.org/10.30909/VOL.03.01.155168

Wanless, V.D., Shaw, A.M., Behn, M.D., Soule, S.A., Escartín, J., Hamelin, C., 2015. Magmatic plumbing at Lucky Strike volcano based on olivine-hosted melt inclusion compositions. Geochemistry, Geophys. Geosystems 16, 126–147. https://doi.org/10.1002/2014GC005517

Werner, C., Rasmussen, D.J., Plank, T., Kelly, P.J., Kern, C., Lopez, T., Gliss, J., Power, J.A., Roman, D.C., Izbekov, P., Lyons, J., 2020. Linking Subsurface to Surface Using Gas Emission and Melt Inclusion Data at Mount Cleveland Volcano, Alaska. Geochemistry, Geophys. Geosystems 21, e2019GC008882. https://doi.org/10.1029/2019GC008882

Wetzel, D.T., Rutherford, M.J., Jacobsen, S.D., Hauri, E.H., Saal, A.E., 2013. Degassing of reduced carbon from planetary basalts. Proc. Natl. Acad. Sci. 110, 8010–8013. https://doi.org/10.1073/PNAS.1219266110

Wieser, P.E., Gleeson, M., 2023. PySulfSat: An open-source Python3 tool for modeling sulfide and sulfate saturation. Volcanica 6, 107–127. https://doi.org/10.30909/VOL.06.01.107127

Wieser, P.E., Iacovino, K., Matthews, S., Moore, G., Allison, C.M., 2022a. VESIcal: 2. A Critical Approach to Volatile Solubility Modeling Using an Open-Source Python3 Engine. Earth Sp. Sci. 9, e2021EA001932. https://doi.org/10.1029/2021EA001932

Wieser, P.E., Lamadrid, H., Maclennan, J., Edmonds, M., Matthews, S., Iacovino, K., Jenner, F.E., Gansecki, C., Trusdell, F., Lee, R.L., Ilyinskaya, E., 2021. Reconstructing Magma Storage Depths for the 2018 Kīlauean Eruption From Melt Inclusion CO2 Contents: The Importance of Vapor Bubbles. Geochemistry, Geophys. Geosystems 22, e2020GC009364. https://doi.org/10.1029/2020GC009364

Wieser, P.E., Petrelli, M., Lubbers, J., Wieser, E., Özaydın, S., Kent, A.J.R., Till, C.B., 2022b. Thermobar: An open-source Python3 tool for thermobarometry and hygrometry. Volcanica 5, 349–384. https://doi.org/10.30909/VOL.05.02.349384

Wilke, M., Klimm, K., Kohn, S.C., 2011. Spectroscopic studies on sulfur speciation in synthetic and natural glasses. Rev. Mineral. Geochemistry 73, 41–78. https://doi.org/10.2138/rmg.2011.73.3

Witham, F., Blundy, J.D., Kohn, S.C., Lesne, P., Dixon, J.E., Churakov, S. V., Botcharnikov, R.E., 2012. SolEx: A model for mixed COHSCl-volatile solubilities and exsolved gas compositions in basalt. Comput. Geosci. 45, 87–97. https://doi.org/10.1016/j.cageo.2011.09.021

Yoshioka, T., Nakashima, D., Nakamura, T., Shcheka, S., Keppler, H., 2019. Carbon solubility in silicate melts in equilibrium with a CO-CO2 gas phase and graphite. Geochim. Cosmochim. Acta 259, 129–143. https://doi.org/10.1016/J.GCA.2019.06.007

Zajacz, Z., Tsay, A., 2019. An accurate model to predict sulfur concentration at anhydrite saturation in silicate melts. Geochim. Cosmochim. Acta 261, 288–304. https://doi.org/10.1016/J.GCA.2019.07.007

Zhang, Y., 1998. Mechanical and phase equilibria in inclusion–host systems. Earth Planet. Sci. Lett. 157, 209–222. https://doi.org/10.1016/S0012-821X(98)00036-3

Zhang, H.L., Cottrell, E., Solheid, P.A., Kelley, K.A. and Hirschmann, M.M., 2018. Determination of Fe3+/ΣFe of XANES basaltic glass standards by Mössbauer spectroscopy and its application to the oxidation state of iron in MORB. *Chemical Geology*, *479*, pp.166-175. https://doi.org/10.1016/j.chemgeo.2018.01.006

1382